REPORT DOCUMENTATION PAGE

Form Approved
OMB No. 0704-0188

PLEASE DO NOT RETURN YOUR FORM TO THE ABOVE ORGANIZATION.

1. REPORT DATE *(DD-MM-YYYY)*	2. REPORT TYPE	3. DATES COVERED *(From - To)*
7/1/2012	Final Technical Report	09/01/2010 -2/29/2012

4. TITLE AND SUBTITLE
Development of an Acetate- or Sugar-fed Microbial Power Generator for Military Bases

5a. CONTRACT NUMBER
N00014-10-M-0231

5b. GRANT NUMBER
N00014-10-M-0231

5c. PROGRAM ELEMENT NUMBER

6. AUTHOR(S)
Dr. Bruce E. Rittmann
Dr. César I. Torres
Dr. Rosa Krajmalnik-Brown
Dr. Sudeep Popat
Dr. Prathap Parameswaran

5d. PROJECT NUMBER

5e. TASK NUMBER

5f. WORK UNIT NUMBER

7. PERFORMING ORGANIZATION NAME(S) AND ADDRESS(ES)
Arizona State University
Office for Research and Sponsored Projects B163
PO Box 873503
Tempe AZ 85287-3503

8. PERFORMING ORGANIZATION REPORT NUMBER
KXS-0049-2

9. SPONSORING/MONITORING AGENCY NAME(S) AND ADDRESS(ES)
Office of Naval Research
Attn: Linda Chrisey ONR 341
875 North Randolph St
Arlington, VA 22203-1995

10. SPONSOR/MONITOR'S ACRONYM(S)
ONR

11. SPONSOR/MONITOR'S REPORT NUMBER(S)

12. DISTRIBUTION/AVAILABILITY STATEMENT
No distribution limitations

13. SUPPLEMENTARY NOTES
N/A

14. ABSTRACT
Military missions often require the transport of fuel, such as diesel, to military bases in remote locations. The delivery of such flammable fuels is very expensive and dangerous, particularly in hostile environments. An ideal fuel source for military missions would be non-flammable, renewable, and readily available. Microbial fuel cells (MFCs) are a new technology in which microbes convert organic compounds (sugars, alcohols, complex wastes) directly into electrical power. Microbial catalysis at the anode opens up the possibility to use non-flammable organic material as a fuel-cell fuel, not just H2, as with a conventional fuel cell.

MFCs have been proven to produce significant power densities (>1 W/m2 of electrode) at a small scale. In our work, we designed a prototype MFC as a module for future large-scale applications that is capable of producing high power densities with minimal potential losses. In order to achieve this goal, we tested various materials, MFC designs, microbial community optimization, and transport limitations. Our results show the need to better optimize ion transport in MFCs, while making significant progress towards achieving an efficient conversion of sucrose to electricity.

15. SUBJECT TERMS
MFCs - Microbial Fuel Cells
ARB - Anode respiring bacteria

16. SECURITY CLASSIFICATION OF:			17. LIMITATION OF ABSTRACT	18. NUMBER OF PAGES	19a. NAME OF RESPONSIBLE PERSON
a. REPORT	b. ABSTRACT	c. THIS PAGE			Bruce E. Rittmann
U	U	U	UU		19b. TELEPHONE NUMBER *(Include area code)*

Reset

Technical Report for the Office of Naval Research

Title: Development of an Acetate- or Sugar-fed Microbial Power Generator for Military Bases

PIs: Dr. Bruce Rittmann, Dr. César Torres, and Dr. Rosa Krajmalnik-Brown

Other Contributors: Dr. Sudeep Popat, and Dr. Prathap Parameswaran

Affiliation: Swette Center for Environmental Biotechnology, Biodesign Institute, Arizona State University

Award #: N00014-10-M-0231

The world is in urgent need of renewable energy sources. Fossil fuel reserves are depleting worldwide, and the harmful effects of their use on global climate are increasingly becoming evident. Fossil fuels dominate the United States' energy portfolio, and thus finding local, renewable sources is a top priority to ensure energy security of our country (U. S. DOE, 2009). Challenges related to energy are also evident in the U.S. military, which consumes 395,000 barrels of oil every day (Warner and Singer, 2009). Transport of fossil fuels to remote places in hostile environments represents a significant cost and security risk to the military.

An ideal fuel for military missions is one that would be readily available, and renewable. In addition, a non-flammable fuel would reduce the risks associated with its transportation. Our project explores one possible solution to this requirement. We investigated the possibility of using microbial fuel cells (MFCs) to generate electrical power at military bases from inexpensive, non-combustible fuels. MFCs are a class of fuel cells in which conversion of energy present in chemical bonds is recovered in usable form without any combustion. In MFCs specifically, bacteria grow on an anode and convert organic fuels to generate an electrical current. The electrons move through a circuit to the cathode where oxygen (O_2) is reduced to water on metal catalysts. Unlike other widely developed fuel cells (e.g., PEM fuel cells) that use hydrogen (H_2), a combustible gas as the fuel, MFCs have the versatility of being able to convert biodegradable organic material.

The concept of MFCs is relatively new and holds great promise for energy recovery from organic materials, especially various kinds of wastes. Figure 0.1 is a schematic of how an MFC works. Inside an MFC, anode-respiring bacteria (ARB) catalyze the conversion of organic matter directly into electricity. ARB form a biofilm on the surface of an electrode (the anode) and transfer electrons to the anode from the oxidation of a variety of electron donors, such as glucose, ethanol, acetic acid, and others (Liu et al., 2005; Logan et al., 2006; Torres et al., 2007). A key concept in an MFC is that ARB transfer electrons to the electrode instead of directly transferring them to a terminal electron acceptor. Therefore, the electrons must pass through a circuit where energy is drawn before they finally reach the cathode, the location where they reduce O_2 to form water. To separate the anode and cathode compartments, a membrane capable of transferring protons (H^+) or hydroxides (OH^-) is usually used; most MFC studies use a proton exchange membrane (PEM) for this purpose (Chaudhuri and Lovley, 2003; Logan et al., 2006), but we use an anion-exchange membrane to obtain important benefits.

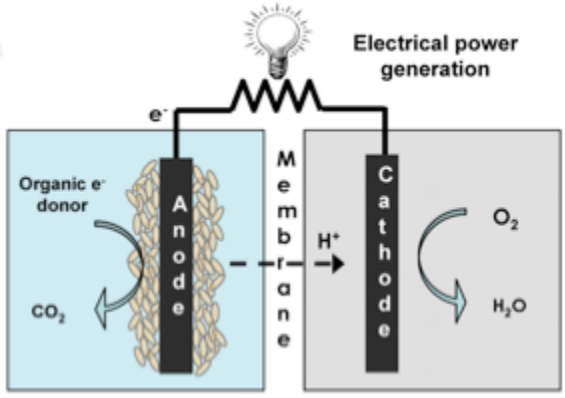

Figure 0.1. *Schematic of the components in an MFC. The anode compartment (left) holds an anode in which anode-respiring bacteria (ARB) grow as a biofilm. In the cathode compartment (right), air is fed to supply O_2 as oxidant. An electron flow from anode to cathode generates electrical power. Ions (expressed as H^+ in the figure) are transported between the compartments to provide electroneutrality through an ion-exchange membrane.*

An MFC is a hybrid between an electrochemical cell and a biofilm reactor. In order to optimize its performance and maximize its efficiency, a novel MFC design that allows bacteria to grow, while minimizing potential losses in the electrical and ionic circuit of the fuel cell, is needed. First, the ARB require a high surface area, as they grow as a biofilm, and have required growth conditions (e.g., water, neutral pH, nutrients) that must be available in the anode compartment. A high ratio of biofilm surface area to MFC volume allows a high output-power density. Second, fuel cells should be developed in a compact design, where the distance between anode and cathode is <1 cm, in order to minimize energy losses. Thus, a main goal for this project was to design an MFC capable of producing high power densities with minimal potential losses.

For military operations, a simple fuel source that is easily consumed by ARB is desirable. In our project, we studied two non-flammable, renewable fuels that are cheap and widely available: acetate and sucrose. We selected these two fuels because of their wide availability in the world market, their relative low cost, and the capability to produce high power densities from them in laboratory MFCs. While both these fuels have low energy density compared to gaseous fuels such as H_2 or CH_4, as well as liquid fuels such as gasoline and diesel (Perlack et al., 2005), they are non-combustible and thus represent a possible cost savings in transportation due to lower safety standards required.

As shown in Figure 0.1, the MFC has various components that must be optimized for its operation. These include: (1) the ARB, which catalyze the fuel oxidation, (2) the anode and

cathode materials, and (3) the ion-exchange membrane. In this project, we targeted optimization of each component of MFCs and then used these components in novel reactor designs that yield high power densities.

Major Achievements of this Project

Described below briefly is the organization of the report and a description of the major achievements made in the design of MFCs.

1) Characterization and selection of anode materials: In this section, we describe our efforts to optimize the anode material for growth of ARB. We tested graphite and stainless steel as possible materials to grow ARB and evaluated current production on both.

2) Characterization and selection of anion exchange membrane: In this section, we describe the various characterizations that we performed on commercially available anion exchange membranes in terms of their resistance to ion transport. We also discuss why it is important to use an anion exchange membrane, as opposed to the more commonly used proton exchange membrane.

3) Construction and performance of first MFC prototype: In this section, we describe the performance of the first flat-plate MFC prototype that we constructed, for which we used acetate as the fuel. We show, using images, how we step-by-step constructed the MFC and how we envision the various components to be used in an efficient design. We also show how the cathode limits the power densities in MFCs, which led to the studies described later.

4) Characterization of anode and Ohmic losses in MECs: In this section, we describe how we used a microbial electrolysis cell (MEC), in which additional voltage is added to overcome any cathodic limitations, to study other components of our design in further detail. This allowed us to study the energy losses at the anode and due to ion transport. We determined that these losses are small, and high current densities can be achieved with minimal energy losses as long as (i) a high surface area electrode is available for ARB to grow on, and (ii) the distance between the anode and the cathode is minimized to <0.5 cm.

5) Identification and characterization of cathodic overpotentials: This section describes the in-depth studies we conducted to determine the reasons leading to cathodic limitations in MFCs. We used platinum catalyst in all our cathodes. We know that platinum catalysts allow current densities that are 2 to 3 orders of magnitude higher in chemical fuel cells. We describe the

importance of the transport of OH^- (a product of the O_2 reduction reaction) in cathode performance, and we show that cathode performance can be improved either by changing some of the materials of construction or selecting a buffer that can be transported rapidly and act as an OH^- carrier out of the cathode surface.

6) Development of co-culture for enhanced energy recovery from sucrose: Efficient ARB such as *Geobacter* sp. use acetate primarily as their electron donor. Thus, to covert a more complex fuel, such as sucrose, additional fermentative bacteria are needed. In this section, we describe our efforts in developing a homo-acetogenic culture that converts sucrose mostly to acetate, which can be further converted to electrical current by *Geobacter* sp. We also show how a co-culture leads to enhanced recovery of electrons (>80%) in an MEC.

This project led to publication of two peer-reviewed journal papers listed below:

1. S. C. Popat, D. Ki, B. E. Rittmann, C. I. Torres (2012). Importance of OH^- transport from cathodes in microbial fuel cells. *ChemSusChem*, 5, 1071-1079.
2. D. R. Bond, S. M. Strycharz-Glaven, L. M. Tender, C. I. Torres (2012). On electron transport through *Geobacter* biofilms. *ChemSusChem*, 5, 1099-1105.

1. Characterization and selection of anode materials:

Several materials have been used successfully as anodes to grow ARB. Carbon-based electrodes are the most popular, and we have extensively used graphite and carbon fibers as anode support for ARB growth in our laboratory (Torres et al., 2008a; Torres et al., 2008c; Lee et al., 2010). Other research groups have used these and other carbon-based materials, such as activated carbon (He et al., 2006). Non-corrosive metals, such as stainless steel and gold, have also been used as an MFC anode (Richter et al., 2008; Dumas et al., 2008).

A main requirement for a good anode material is to provide a high surface area for ARB biofilms to grow. Maximizing ARB growth area maximizes volumetric current densities in MFCs. Carbon fibers are lightweight, inexpensive, and have a 7-12 μm diameter, which allows a high surface-to-volume ratio. However, they are not as conductive as metal alloys such as stainless steel, and, thus, a current collector is required to build the anode. Instead, stainless steel fibers could possibly serve as an anode material, also allowing more efficient current collection. Although stainless steel fibers are more expensive and heavier than carbon fibers, we hypothesized that they would allow high current densities at lower potential losses due to their high conductivity, if ARB are able to grow well on them. Therefore, we evaluated carbon and stainless steel anodes in the first phase of this project to select the best material for MFC modules.

We compared the performances of acetate-fed microbial electrolysis cells (MECs) with graphite rods and stainless steel meshes, selected as simple anodes to rapidly test the affinity of ARB towards them. We selected meshes made from 316-grade stainless steel for these studies. We conducted several trials with the MECs, similar to as we have done in the past (Torres et al., 2008b; Parameswaran et al., 2009), and the performance of one set of MECs is reported in Figure 1.1. As expected with graphite rod anodes, we were able to achieve current densities of ~11 A m_{an}^{-2} at a poised anode potential of -0.4 V vs. Ag/AgCl (Figure 1.1(a)) when inoculated with anaerobic digested sludge as inoculum. This is consistent with our previous results using graphite as anode material, wherein we have been able to enrich for *Geobacter* spp. and obtain similar current densities at this poised potential (Torres et al., 2009). We were unable to enrich for efficient ARB from the same anaerobic digested sludge inoculum using a stainless steel mesh anode at a poised potential of -0.4 V vs. Ag/AgCl (data not shown). When we used enriched ARB cultures as inoculum in stainless steel anode MECs, we observed current generation, but current densities were an order of magnitude lower than for graphite rod MECs (Figure 1.1 (b)).

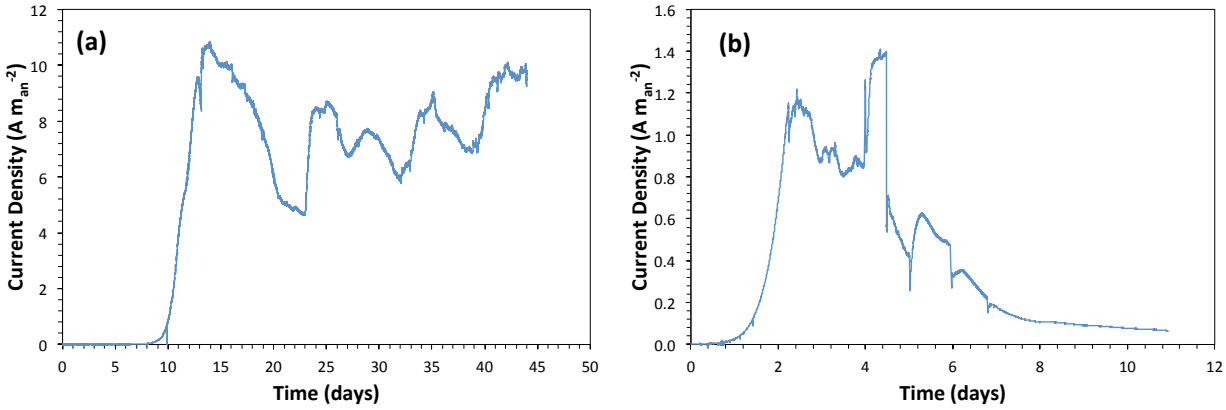

Figure 1.1. *Performance of acetate-fed MECs with (a) a graphite rod anode and (b) a stainless steel mesh anode. The anode potential was poised at -0.4 V vs. Ag/AgCl. The graphite rod anode MEC was operated in batch more until day 22 and then continuously fed for the rest of the duration. The MEC with the stainless steel anode was operated in batch mode through the reported duration of operation. Note the different scales on the vertical axes.*

We postulated that the stainless steel surface hindered the enrichment for ARB efficient in extracellular electron transport (EET) using a conductive biofilm matrix. We thus conducted cyclic voltammetry (CV) scans on one set of graphite rod and stainless steel mesh anode MECs to compare the possible EET mechanisms between the two. These CV scans are shown in Figure 1.2. The curve for the graphite rod anode MEC (Figure 2.2 (a)) fits the Nernst-Monod

model (fitting not shown) (Marcus et al., 2007; Torres et al., 2008b). This successful model fit, in combination with the high current densities, confirms the use of a conductive biofilm matrix for EET. The E_{KA} value determined from the curve fitting was -0.43 V vs. Ag/AgCl; this is consistent with values determined for *Geobacter* sp. (Torres et al., 2008b).

Contrastingly, the curve for the MEC with the stainless steel mesh anode (Figure 2.2 (b)) did not fit the Nernst-Monod model, even when using an enriched inoculum. We believe that stainless steel may have induced a change in the EET mechanism. It is known that OmcZ, an outer membrane cytochrome in *Geobacter* spp. is required for efficient EET and optimal current generation (Inoue et al., 2011). We suspect that stainless steel inhibited the functioning of this cytochrome, either due to its inherent chemical properties or leaching of metal ions, such as nickel and chromium that could have interacted negatively with important proteins. We are interested in continuing to evaluate the performance of stainless steel anodes to gain further insight into the reasons for the poorer performance of ARB. However, given the short timeline of the project, we moved forward with the use of graphite fibers as anodes for the MFC modules.

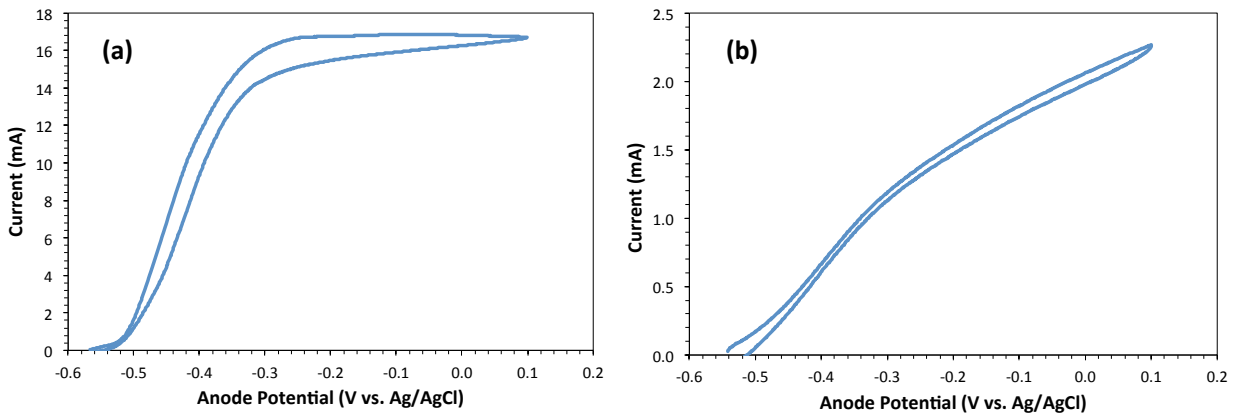

Figure 1.2. *CV scans of acetate-fed MECs with (a) graphite rod anode and (b) stainless steel anode, performed after pseudo steady state. The scan rate was 1 mV* s^{-1}*. Note the different scales on the vertical axes.*

2. Characterization and selection of anion exchange membrane:

The ion exchange membrane serves two purposes in an MFC. The first is to avoid crossover of O_2 from the cathode chamber to the anode chamber, where anaerobic conditions need to be maintained for optimum growth and activity of efficient ARB. Avoiding O_2 crossover also avoids

the growth of aerobic heterotrophic bacteria that would decrease the Coulombic efficiency by diverting electrons present in the substrate towards the reduction of O_2. The second is to allow efficient and preferential transport of ions from the anode chamber to the cathode chamber, or *vice versa*, to maintain electroneutrality.

It has been shown in the past that using a proton exchange membrane (PEM), which needs to transport H^+ produced from anode respiration to the cathode chamber, leads to the development of pH gradients between the anode and the cathode chambers, with the cathode chamber pH shown often to reach close to 13 (Rozendal et al., 2007). From the Nernst equation, it is known that every pH unit that the cathode pH is higher than the anode pH leads to a loss of ~60 mV of thermodynamic potential at room temperature. The underlying reason for this pH imbalance is that the anode chamber contains other cations such as Na^+ and K^+, which are present in such high concentrations (10-100 mM) in comparison to H^+ (~10^{-4} mM), that electroneutrality is maintained through transport of these ions instead of H^+.

Researchers have investigated the use of other membranes, such as anion exchange membranes (AEMs) (Torres et al., 2008c), bipolar membranes (Ter Heijne et al., 2006), and simple filters/insulators (Kim et al., 2007), to avoid the issue of pH imbalance between the anode and the cathode chambers. Of these, AEMs have been found to perform well (Harnisch et al., 2008; Sleutels et al., 2009). When using an AEM to separate the anode and the cathode, electroneutrality is maintained by transport of OH^- from the cathode chamber to the anode chamber, either directly or via anionic buffers such as phosphate and carbonate species. The use of AEMs has consistently shown to reduce the pH imbalance between the anode and the cathode chambers in various MXCs, and we thus decided to use AEMs in developing our MFC prototypes.

While the use of AEMs to transport OH^- from the cathode chamber to the anode chamber has been proposed since 2007, a systematic study of various commercially available AEMs, in terms of their resistance to ion transport in conditions relevant to MFCs, has not been performed. Thus, we used electrochemical impedance spectroscopy (EIS) to characterize five commercially available AEMs (Table 2.1) in this aspect. For these experiments, we used electrochemical cells containing two chambers filled with relevant solutions (individually 100 mM PBS and 100 mM $NaHCO_3$), with stainless steel rod electrodes, and separated by the membrane to be characterized. We performed EIS on the cell with one stainless steel rod as the working electrode, the other as the counter and reference electrode, and at 200 MHz and amplitude of 0.02 V. This allowed measurement of the Ohmic loss between the two electrodes for various membranes. We also performed EIS analysis without a membrane to get the background

Ohmic loss from the liquid solutions used, thus making it possible to determine the resistance to ion transport only from the membrane.

Table 2.1. *List of membranes tested, including their supplier and physical properties.*

Membrane	Supplier	Thickness	pH Stability
AMI-7001	Membranes International, USA	0.50-0.51	1-10
Excellion I-200	SnowPure, USA	0.32-0.34	NR
Fumasep FAA	FuMa-Tech, Germany	0.13-0.15	6-13
Fumasep FAB	FuMa-Tech, Germany	0.10-0.13	0-14
A201	Tokuyama, Japan	0.028	0-14

We show in Figure 2.1 the resistances to ion transport from different membranes in 100 mM PBS (Figure 2.1 (a)) and 100 mM $NaHCO_3$ (Figure 2.1 (b)). AMI-7001 is a standard AEM that is used in various laboratory MXC studies (Parameswaran et al., 2009). We found that, of all the membranes we tested, AMI-7001 had among the largest resistances to transport of anions. The FAA, FAB, and A201 membranes provided significantly less resistance to anion transport compared to the AMI-7001 and I-200 membranes.

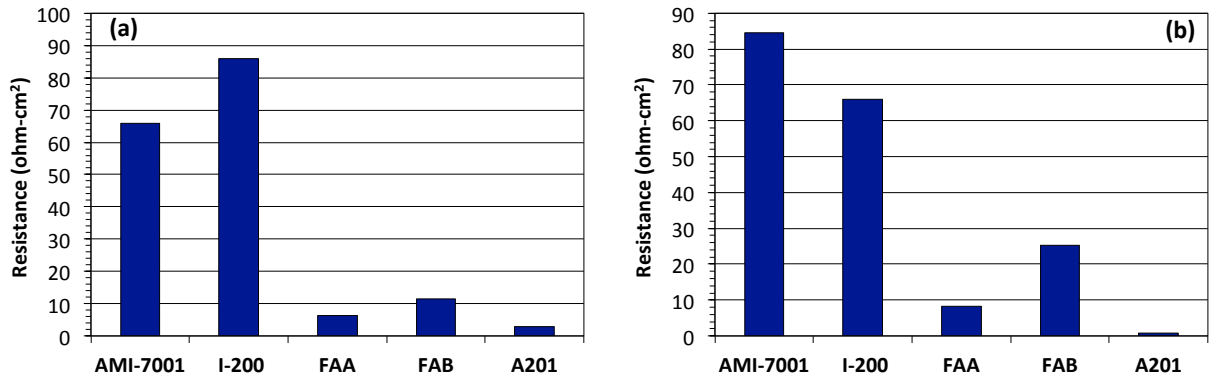

Figure 2.1. *Resistances of various membranes tested in (a) 100 mM PBS, and (b) 100 mM $NaHCO_3$.*

We selected A201 as the membrane to use in the MFC prototypes, since it provided the least resistance to anion transport irrespective of the electrolyte. Since A201 also has a much wider range of pH stability compared to AMI-7001, we anticipated that A201 also would be more stable over long-term operation.

3. Construction and performance of first MFC prototype:

Based on the materials tested (described in sections 1 and 2) and the concepts from fuel cell designs, such as minimizing the distance between the anode and the cathode, we constructed our first flat-plate MFC prototype (Figure 3.1). Here we describe the salient features of our design. For the cathode, we decided to follow the guidelines that have been developed for construction cathodes for PEM fuel cells. The cathode design begins with a serpentine flow field (Figure 3.1 (a)), which is constructed from a graphite block that also acts as a current collector. This flow field allows efficient transport of O_2 to the active cathode catalyst sites. It also allows removal of excess moisture that may be present on the cathode. While we conducted some experiments described below using this serpentine flow field, including the performance of the MFC we report below, we later discovered that the flow field was not essential in maintaining cathode performance. The flow rate of O_2 in the flow field hardly affected the current densities, and an open-air cathode typically achieved the same current densities. Thus, the use of this serpentine flow field could be excluded while scaling up our design. However, this would require the use of an efficient current collector. In the laboratory, a stainless steel plate contacting the cathode at its edges (photo not shown) sufficed, but for larger systems, concepts such as building the cathode around a stainless steel mesh developed by Zhang et al. (2010) appear promising.

Next we describe the cathode itself, which is shown in Figure 3.1 (b). The cathode consists of a carbon cloth support. On one side of the cloth, which faces the serpentine flow field or is open to air, a paste of carbon and a hydrophobic polymer (in our case polydimethylsiloxane, or PDMS) is applied. The cloth together with this hydrophobic carbon layer is referred to as a gas diffusion layer (GDL). The GDL allows efficient transport of O_2 to the catalyst sites by ensuring that O_2 diffusion is not limited by "flooding" of the cathode. On the other side of the cloth, which faces towards inside the reactor, the catalyst layer is coated. We used Pt/C as the catalyst, at loadings of 0.5 mg Pt/cm^2. The Pt/C powder is mixed with an ionomer to form a paste, which is used to paint the catalyst later on the cloth. The ionomer allows transport ions,

thus maintaining charge neutrality. We used Nafion as the ionomer in the first set of designs we describe here, but evaluated its use critically later on (see section 5).

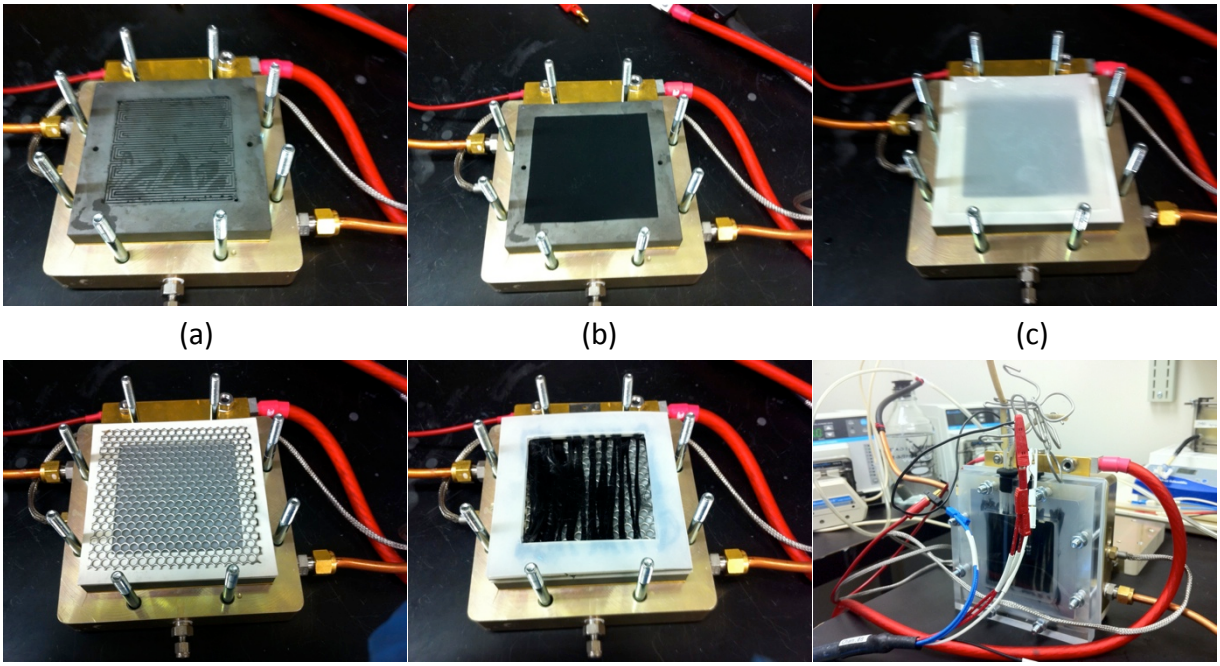

Figure 3.1. *Photographs of the first flat-plate MFC prototype we developed at various stages of construction. See the text for details.*

From the studies described in section 2, we selected A201 as the AEM of choice in the MFC design. The membrane is placed immediately next to the cathode (Figure 3.1 (c)) to minimize distance between the anode and the cathode. On the side of the membrane opposite to the one facing the cathode, we placed a stainless steel mesh (Figure 3.1 (d)). In other studies that we have done with various MFC designs, we had noted that the flow of anions from the cathode to the anode chamber causes the membrane to deform, bending towards the anode side. This deformation leads to increased Ohmic losses. Others also have seen this phenomenon (Zhang et al., 2010). We thus used the mesh to support the membrane against the cathode in order to prevent membrane deformation. In subsequent trials (not reported here), we replaced the stainless steel mesh with a plastic mesh to avoid corrosion.

After the mesh to support the membrane, we placed the anode, which consisted of a titanium frame acting as a current collector, with wound carbon fibers to allow enough anode area for ARB to grow (Figure 3.1(e)). The anode chamber was then closed with a Plexiglas frame. A photograph of the final set-up is shown in Figure 3.1 (f). In our prototypes, we used an anode

volume of 100 mL, but this can be easily adjusted to achieve required rates of power production.

We conducted three trials using this design, replacing certain elements (e.g., the mesh material to support the membrane) in each iteration. We report here results from only one of the trials. In all trials, we used acetate as the electron donor for ARB and inoculated the MFCs with a *Geobacter* sp.-enriched inoculum from other operating reactors in our laboratory. We used a phosphate-buffered medium for growing ARB, which has a conductivity of 15.5 mS/cm. We started all MFCs in batch-mode, and switched them to continuous mode once we observed current production, at a hydraulic retention time of 4-6 hours. We operated all MFCs with a potentiostat, with the anode potential poised at -0.3 V vs. Ag/AgCl. We continuously monitored the current production, as well as the cathode potential, to determine power densities. We show in Figure 3.2 below, the performance of one of the prototypes we constructed.

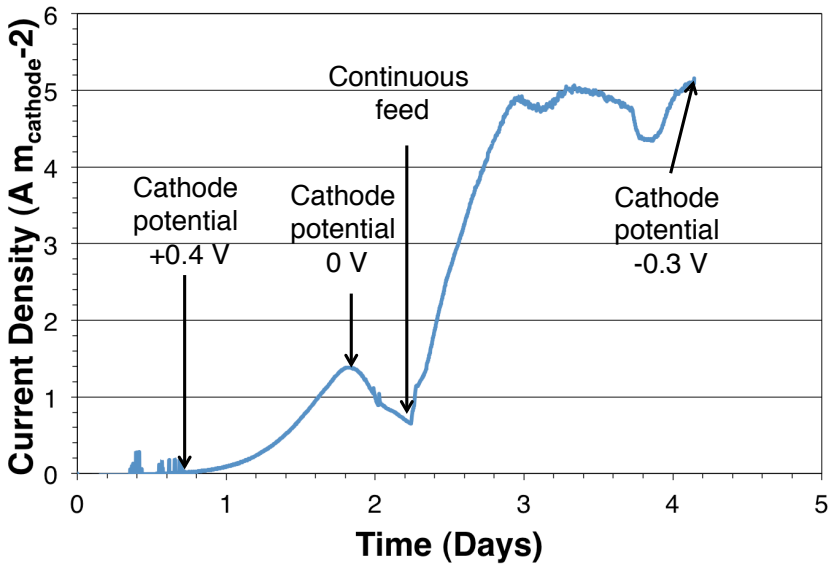

Figure 3.2. *Performance of one of our MFC prototypes in terms of current density vs. time.*

Using an active inoculum, we observed current production within one day of starting the MFC. The cathode open circuit potential (OCP, i.e., when current production had not begun) was +0.4 V vs. Ag/AgCl. This is lower than the expected theoretical OCP for oxygen reduction of +0.54 V vs. Ag/AgCl (or +0.81 V vs. SHE). In other trials, the OCP was as low as ~+0.15 V vs. Ag/AgCl, suggesting that roughly 0.2-0.4 V of theoretically available voltage was lost even without any current production, possibly due to mixed potential arising from possible side reactions. The current density increased with time up to ~1.5 A/$m_{cathode}^2$, after which there was a decrease

due to consumption of all acetate, since the anode volume was very small. We switched the MFC to continuous mode thereafter, and the current density increased to up to 5 A/m^2.

The continuous measurement of the cathode potential showed that, by 1.5 A/m^2, the cathode potential had already decreased to 0 V vs. Ag/AgCl. This represents a power density of ~450 mW/m^2. The maximum power density was achieved at a current density of ~4 A/m^2, when the cathode potential was ~-0.1 V vs. Ag/AgCl, which amounts to a power density of ~800 mW/m^2. These power densities are on the lower end of what has been observed in laboratory studies in the past 3-4 years in ours (Torres et al., 2008c), as well as other groups (Logan et al., 2008). By 5 A/m^2, the cathode potential reached -0.3 V vs. Ag/AgCl, at which point no power was being produced. Since the anode potential was set at -0.3 V vs. Ag/AgCl, only ~0.25 V was lost to anode potential losses (anode OCP should be ~-0.55 V vs. Ag/AgCl) at the highest current densities, while ~0.85 V was lost at the cathode. Note that this also includes the Ohmic loss, which we estimate to be <0.1 V, unless ionic contact between the membrane and the cathode was poor. This tells us that the power densities in our MFC design were limited by the cathode reaction. Although this was surprising, since Pt/C catalyst allows obtaining current densities that are 100-1000 times higher in chemical fuel cells, we acknowledged that cathodic limitations have been increasingly determined as a key parameter in scaling up MFCs based on various other studies in the last few years (Cheng and Logan, 2006; Rismani-Yazdi et al., 2007; Fan et al., 2007). Thus, we decided to focus on understanding the MFC cathodic limitations in more detail (Section 5). We believe that solving cathodic limitations will be an important step in gearing MFCs towards scale-up and practical applications.

4. Characterization of anode and Ohmic losses in MECs:

Before conducting studies on the cathode, we determined the anode and Ohmic losses in our design. To do this, we conducted further studies in microbial electrolysis cells (MECs). In MECs, O_2 is excluded from the cathode, and instead water is reduced to H_2 gas. The absence of O_2 at the cathode is advantageous to characterize the anode, in which ARB could be inhibited by the O_2 diffused from the cathode. This configuration requires ~0.14 V of energy input to make the H_2-evolution reaction on the cathode thermodynamically favorable. In reality, additional voltage needs to be applied to overcome potential losses at the anode, at the cathode, and due to ion transport (i.e., Ohmic losses). By tracking the applied voltage as a function of current density and using various electrochemical techniques, we could separate the contribution of each to the total applied voltage. For these studies, we used an MEC that included the same anode and membrane we used in our MFC prototypes (see Figure 4.1 for photograph of MEC),

as well as the same design features (for e.g. short distance, i.e. <0.5 cm, between the anode and the cathode).

Figure 4.1. *Photograph of MEC used to study anode and Ohmic losses for our electrode configuration.*

In the flat-plate MEC, we were able to achieve volumetric current densities of up to 500 A/m_{anode}^3. Note that we use the current density normalized to anode volume in the discussion here, as opposed to that normalized to cathode area, since with improving the anode performance and reducing Ohmic losses, the primary aim is to obtain high anodic volumetric current densities. Once the ARB biofilm had fully grown and a steady-state current density was reached, we performed cyclic voltammetry (CV) on the biofilm to get insights into anode potential losses. We show the CV below in Figure 4.2. The CVs showed typical Nernst-Monod behavior of ARB kinetics, with the maximum current densities achieved by an anode potential of -0.35 V vs. Ag/AgCl. This represents an anode potential loss of only 0.2 V, which agrees with our previous studies described in this report. The maximum volumetric current density we report here also is among the highest reported, confirming that using a large surface area anode allowed reaching high current densities, while minimizing additional potential losses.

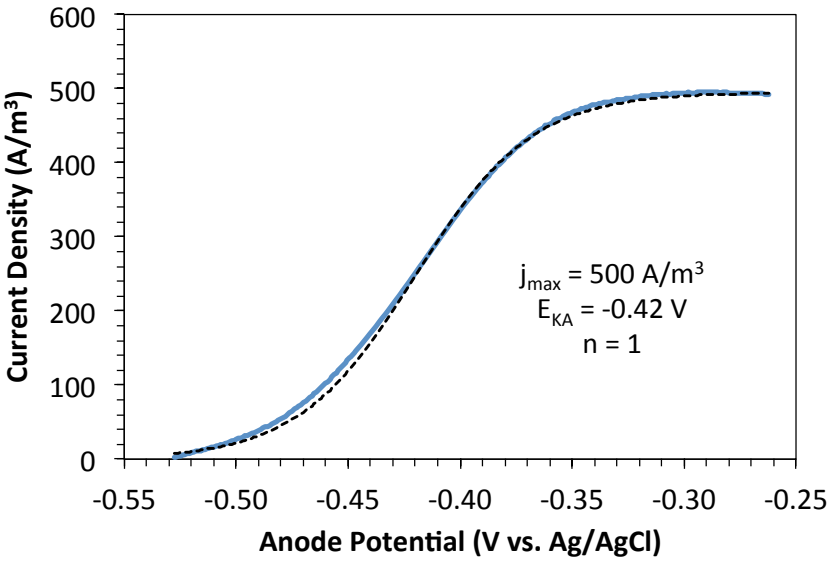

Figure 4.2. *Cyclic voltammetry of MEC ARB biofilm.*

We further characterized MEC performance by using additional electrochemical techniques. First we performed EIS analysis at open circuit to determine the Ohmic loss. It was negligible, since our design places the anode and the cathode <0.5 cm apart and also because we used a relatively high conductivity phosphate buffer on the anode chamber. We then performed chronoamperometry, changing the anode potential from open circuit to -0.3 V vs. Ag/AgCl, while recording current density, cathode potential, and cathode liquid pH. We then used this information to separate the various components of applied voltage, and these are shown in Figure 4.3. We show that anode and Ohmic potential losses contribute together only a small fraction of the total applied voltage (or potential losses). Although we separate pH losses from cathode losses in Figure 4.3, we show in section 5 that these are typically also associated with the cathode, and thus even in MECs, we conclude that cathode losses result in the highest fraction of applied voltages at a given current density. Thus, EIS confirms that our design helps ensure that anode and Ohmic potential losses are minimized. It also confirms the importance of finding ways in which we can we can improve cathode performance.

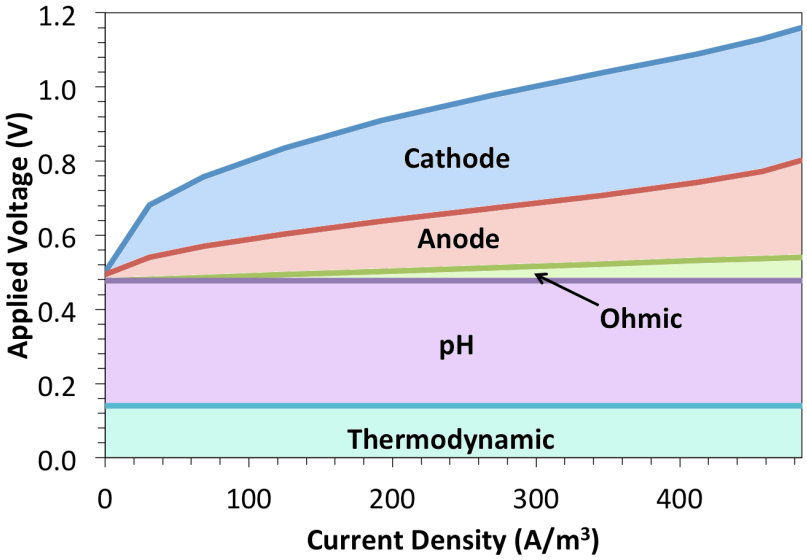

Figure 4.3. *Applied potential as a function of current density in the MEC.*

5. Identification and characterization of cathodic overpotentials*:

Because our first prototype MFC was limited by cathode performance, we decided to investigate the reasons for this limitation. In general, it has become evident over the last few years that MFCs are more likely to be limited, in terms of maximum achievable power densities, by cathodic potential losses (Zhao et al., 2006; Rozendal et al., 2008; Rismani-Yazdi et al., 2008). Our aim was thus to understand the underlying reasons for cathodic potential losses at typical current densities (0-20 $A/m_{cathode}^2$) and, as a direct outcome, evaluate solutions to overcome these losses.

It is often suggested that cathodes in MFCs are limited because of the difficulty providing protons, a supposed reactant at the active catalyst sites, at typical conditions, such as neutral pH. This assumes that the oxygen reduction reaction (ORR) proceeds as follows, based on proton exchange membrane (PEM) fuel cells:

$O_2 + 4\ e^- + 4H^+ \rightarrow 2H_2O$

However, cathodes in MFCs are subjected to significantly different conditions than in PEM fuel cells, e.g., direct contact with an electrolyte at neutral pH. Thus, we first analysed whether this

* *The work described in this section led to the publication: S. C. Popat, D. Ki, B. E. Rittmann, C. I. Torres (2012). Importance of OH^- transport from cathodes in microbial fuel cells. ChemSusChem, 5, 1071-1079.*

minimal availability of protons as reactant can actually support the cathodic current densities typically observed in MFCs.

If the ORR proceeds on cathodes in MFCs through the use of protons as a reactant, the flux of protons through the catalyst layer and the diffusion boundary layer, of the cathode, has to be sufficient enough to support the current densities of 5-10 A/m^2 that are usually observed. This transport of protons occurs mainly through diffusion. Using typical values for the diffusion boundary layer thickness, we computed a maximum flux of protons in the order of 10^{-10} - 10^{-9} $mmoles/cm^2 \cdot s$, which corresponds to current densities in the order of 10^{-3} - 10^{-2} A/m^2. This is 100-1000 times lower than current densities typically observed; thus, we conclude that ORR does not proceed in MFCs as it does in PEM fuel cells. It must occur through the alternative mechanism, shown below, which is dominant in alkaline fuel cells (Varcoe et al., 2005):

$O_2 + 4\ e^- + 2H_2O \rightarrow 4OH^-$

We hypothesized that cathodes in MFCs are limited because of poor OH^- transport out of the cathode into the bulk electrolyte. Inability to rapidly transport OH^- from the active catalyst sites to the bulk liquid will result in an increase its local concentration, leading to concentration over-potential. From the Nernst equation, every increase in one pH unit decreases the redox potential for the ORR by ~59 mV (at room temperature), and thus we postulated that a significant amount of cathodic potential loss at typical current densities is likely associated with an increase in the local cathode pH.

The first reason for this limitation stems from the anion-conduction properties of the catalyst binder used for creating a three-phase boundary for the ORR. As an extrapolation from its use in PEM fuel cells, Nafion has been the binder of choice in cathodes in many MFCs (Cheng et al., 2006). However, Nafion contains sulfonate moieties that are efficient in transporting cations, but provide significant resistance to transport of anions, including OH^- (Piela et al., 2006) Buffers, such as phosphate and carbonate species, that would help transport OH^- out of the cathode would also be transport-limited in Nafion. Second is the lack of sufficient agitation, which results in a thicker diffusion boundary layer.

We decided to confirm that OH^- transport limits cathode performance. For this, we obtained a series of cathode polarization curves under different conditions in a gas-diffusion half-cell. We prepared cathodes (9 cm^2) from 30% wet-proofed carbon cloth gas-diffusion boundary layers coated with a microporous carbon layer (CMPL) on one side (Electrochem Inc., USA). We prepared catalyst ink using 0.5 g of 30% Pt/C powder (Electrochem Inc., USA) mixed in 5 mL of 5% ionomer in iso-propanol solution (Nafion, Sigma-Aldrich, USA, or AS-4, Tokuyama

Corporation, Japan) by sonication for 30 minutes and magnetic stirring for 24 h, as binder, and applied it the side of cathodes opposite to the CMPL, using a paint brush. We used a Pt loading of 0.5 mg/cm^2 on all the cathodes. We constructed gas-diffusion half-cells (3 cm × 1.8 cm × 3 cm) as Plexiglas chambers of ~16 mL volume, closed at one end. We placed the cathodes at the other end with the catalyst-coated side facing inside (towards the solution) and the MPCL outside (towards air). We used a saturated calomel electrode (+0.244 V vs. SHE) as the reference electrode and placed it inside the cells at a distance of 5 mm from the cathode. We used a stainless steel rod as the counter electrode (~9 cm^2, 5 mm diameter). We performed linear sweep voltammetry (LSV) on cathodes at 30°C using a potentiostat (Princeton Applied Research, USA) at a scan rate of 1 mV/s. We performed i-R correction for all LSVs to correct for the Ohmic loss between the reference electrode and the cathode, using an average Ohmic loss as measured from ~20 impedance spectroscopy measurements at 100 kHz with an amplitude of 10 mV.

We first obtained polarization curves for cathodes constructed with Nafion binder in unbuffered 100 mM $NaClO_4$ solution at pH 7.5, 10.8, or 13 (Figure 5.1 (a)). It is evident that the cathode in pH 7.5 had the largest potential losses, particularly at low current densities. The difference in potential for the cathode in pH 7.5 vs. the cathodes in higher pH was only maintained at current densities <1 A/m^2, indicative of high potential losses at low current densities. These losses also decreased with increasing bulk liquid pH, indicating that they are related directly to the concentration gradient for OH^- between the bulk liquid and the cathode. Eventually, all cathodes converged to the same potential at high current densities, suggesting that all of them reach the same local pH, irrespective of the bulk liquid pH. This experiment provides the first indication of the importance of OH^- transport from cathodes. Using the polarization curve for the cathode in pH 13, we determined j_0 (i.e., the exchange current density) and α (i.e., the charge transfer coefficient), both values being related to catalyst properties, as 9.5×10^{-8} A/cm^2 and 0.195, respectively. Next, we used the Butler-Volmer equation with the j_0 and α values to predict the response of the cathode in pH 7.5 if it were not OH^- transport limited. We show this in Figure 5.1(b). It is evident that the actual response includes additional overpotential, which has to be related to OH^- transport limitations. We also fit the experimental curve to the Butler-Volmer equation that includes diffusion limitation to obtain the local cathode pH as a function of the current density, which increased to >11 very rapidly at current densities <1 A/m^2 and at 10 A/m^2 was >12.5. This represents a potential loss of >300 mV, or >50% of all cathodic potential losses typically observed in this range of current density.

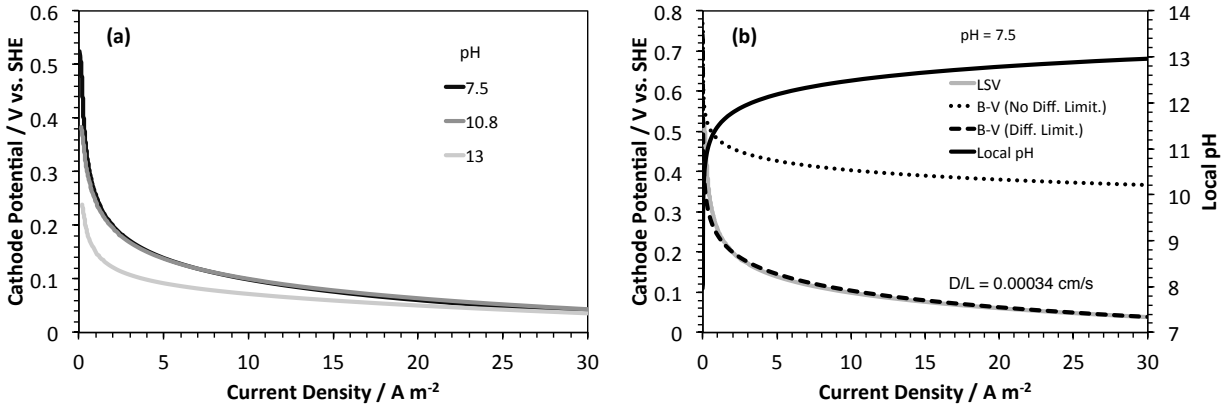

Figure 5.1. *(a) Polarization curves of Pt-based gas diffusion cathodes constructed with Nafion binder in 100 mM $NaClO_4$ solution at different pH. (b) Comparison of polarization curve of Pt-based gas diffusion cathode constructed with Nafion binder in 100 mM $NaClO_4$ solution at pH 7.5 with curves predicted from the Butler-Volmer equation without and with OH^- diffusion limitation, and the predicted local cathode pH as a function of current density resulting from OH^- diffusion limitation.*

While the above experiments were performed in unbuffered solutions, a buffer is typically used in MFCs to maintain the bulk liquid pH closer to neutral. This buffer could also help in transporting OH^- from the cathode to the bulk liquid. Thus, we obtained polarization curves for cathodes constructed with Nafion binder in 100-mM phosphate buffer. Similar to the above experiments, we performed these experiments in buffer solutions with different pH, ranging from 7.2 to 12.9, but we show only the polarization curve in pH 7.2 in Figure 5.2. We also compare the experimentally obtained polarization curve of the cathode in pH 7.2 with the theoretical non-diffusion controlled response in pH 7.2, as determined from the Butler-Volmer equation. The difference between the two provides a measure of potential losses related to increased local cathode pH. At a current density of 10 A/m^2, this difference was >0.3 V, suggesting that the local cathode pH was already ~5 units higher than the bulk liquid pH. Potential losses related to OH^- transport limitation were smaller at low current densities (<5 A/m^2), but still represented a significant fraction. For example, potential loss related to OH^- transport limitation was ~0.15 V at 4 A/m^2, corresponding to a local cathode pH of ~9.7. This pH represents the tail end of where a favourable concentration gradient could exist for OH^- transport through deprotonation of $H_2PO_4^-$ to HPO_4^{2-}.

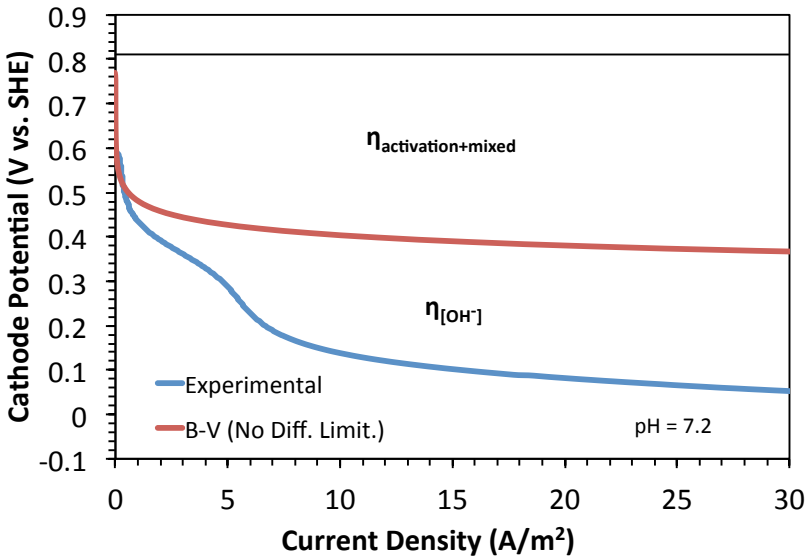

Figure 5.2. *Comparison of polarization curve of Pt-based gas-diffusion cathode constructed with Nafion binder in 100 mM phosphate buffer at pH 7.2 with curves predicted from the Butler-Volmer equation without OH^- diffusion limitation.*

Having established that Nafion provides significant resistance to OH^- transport, either directly or through phosphate buffer as OH^- carrier, we hypothesized that replacing Nafion with an anion-conductive polymer will result in improved cathode performance. Several polymers containing quaternary ammonium moieties have good anion exchange capacity and are available from applications in anion exchange membrane (AEM) fuel cells (Varcoe et al., 2006; Fang et al., 2006; Xiong et al., 2008). We selected one of these, AS-4 (Tokuyama Corporation). We obtained polarization curves for cathodes constructed with AS-4 binder in 100-mM phosphate buffer at pH 7.2 and compared these to those for cathodes constructed with Nafion binder. We show this comparison in Figure 5.3. Compared to the cathodes with Nafion binder, potential losses for the cathode with AS-4 binder were lower. Since we expect activation-related overpotentials to be the same for both cathodes, the improved performance of the cathode with AS-4 binder is a direct result of improved OH^- transport, either directly or through improved transport of the anion buffer species. Within the range of current densities typically observed in MFCs, potential losses for the cathode with AS-4 binder were up to 157 mV lower than for the cathode with Nafion binder, indicating significant improvement in anion transport. Considering this result, we suggest that the use of Nafion as the cathode catalyst binder in MFCs be replaced with anion conductive binders like the one we used here.

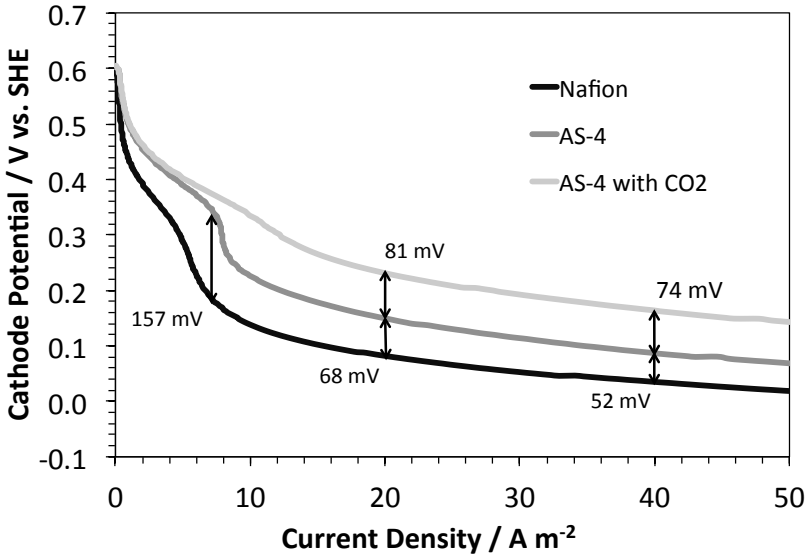

Figure 5.3. *Comparison of polarization curves of Pt-based gas-diffusion cathode constructed with Nafion and AS-4 binders, the latter with and without CO_2 feed to the cathode, in 100 mM phosphate buffer at pH 7.2.*

The maximum savings of 157 mV at 7.5 A/m^2 suggests that the local cathode pH was ~2.6 units lower with the AS-4 binder. Since the cathode with the Nafion binder was close to a local pH 12 at this current density (as we determined previously), the local cathode pH with AS-4 binder was ~9.4. This still represents a significant remaining potential loss related to OH^- transport (~140 mV) and, thus, additional opportunity for improving cathode performance.

A second way to improve cathode performance would be through providing additional buffer in the form of CO_2. We have shown in the past that adding CO_2 to the cathode chamber in MFCs containing a membrane helps in transporting OH^- across the membrane (Torres et al., 2008c). H_2CO_3 (hydrated CO_2) would deprotonate to HCO_3^-, thus acting as an OH^- carrier. The advantage of providing CO_2, especially to gas-diffusion cathodes, is that it can be delivered directly to the catalyst sites through the gas diffusion boundary layer, compared to phosphate buffer that suffers from the same diffusion limitations as OH^-. Also, the second pK_a of the CO_2 buffer system is 10.3, and this would allow maintaining a lower cathode pH at high current densities than phosphate, through OH^- transport via the HCO_3^-/CO_3^{2-} couple.

We obtained polarization curves for the cathodes constructed with AS-4 binder with CO_2 feed (5% mixture with air) as well (Figure 5.3). It is apparent that CO_2 addition did not significantly help in the region of low current density (< 5 A/m^2), since phosphate already was partially aiding OH^- transport. However, CO_2 addition resulted in lower potential losses at the higher

current densities. Compared to the cathode with Nafion (and no CO_2), potential losses were ~120-140 mV lower for the cathode with AS-4 with CO_2 addition, thus representing a local cathode pH close to 10. We thus conclude that enhanced OH^- transport was occurring through the deprotonation of H_2CO_3 to CO_3^{2-}.

Since we found that the cathode performance depended primarily on the pK_a of the buffer used, we explored the use of ammonium (NH_4^+) as a sustainable buffer for improving cathode performance in MFCs. While this might not be a practical application for the purposes of developing a microbial power generator for naval bases, the use of NH_4^+ as buffer could be feasible for treatment of waste streams already containing high NH_4^+ concentrations. The NH_4^+/NH_3 couple has a pK_a of ~9.2, suggesting that it should be possible to maintain the local cathode pH in MFCs in the range of 8.5-10 using NH_4^+ as a buffer, thus further reducing potential losses. To compare the performance of cathodes in NH_4^+ buffer against other buffers, we obtained polarization curves for cathodes constructed with Nafion binder in 50 mM of various solutions (Figure 5.4). As expected, the cathode overpotential in 50-mM unbuffered solutions (NaCl) increased rapidly, even at low current densities, as a result of an increase in the local cathode pH. Our previous analysis suggests that, by 2 A m^{-2}, the local cathode pH already increases by 4-5 pH units in the absence of a buffer, thus representing a significant Nernstian concentration overpotential of ~300 mV due to local accumulation of OH^-. In contrast, the cathode overpotential to reach current densities of up to 5 A m^{-2} was lower in PBS. This was a result of buffering of pH in the range of 7.2-9, which represents the tail end of where $H_2PO_4^-$ deprotonates with OH^-. Beyond this current density, the rate of production of OH^- surpassed the rate of transport of $H_2PO_4^-$, which encountered transport resistance in the catalyst layer due to the use of Nafion as the catalyst binder. Bicarbonate buffer did not significantly help in buffering close to the pK_a of the HCO_3^-/CO_3^{2-} couple of ~10.3, but this could be due to its poor transport properties in Nafion.

In comparison to phosphate and bicarbonate buffers, the overpotentials in NH_4Cl and NH_4HCO_3 were lower at high current densities (>5 A m^{-2}). This confirms our hypothesis that NH_4^+ helped to maintain a lower local cathode pH. Up until 5 A m^{-2}, the cathode in PBS performed better than in NH_4Cl and NH_4HCO_3 because of the buffering effect of phosphate in the pH range of 7.2-9. However, current densities up to 25 A m^{-2} were sustained in NH_4^+ solutions without the LSVs showing an inflection resulting from transport limitation. This likely was an effect of using Nafion as the catalyst binder, since Nafion is efficient in transporting cations, such as NH_4^+. We had shown before that replacing Nafion as the binder with an anionomer can help improve cathode performance when using phosphate or bicarbonate as buffer, but for NH_4^+ buffer,

Nafion is a preferable binder. The higher diffusion coefficient for NH_4^+, compared to the other buffers, also increases its relative transport rates to the cathode surface.

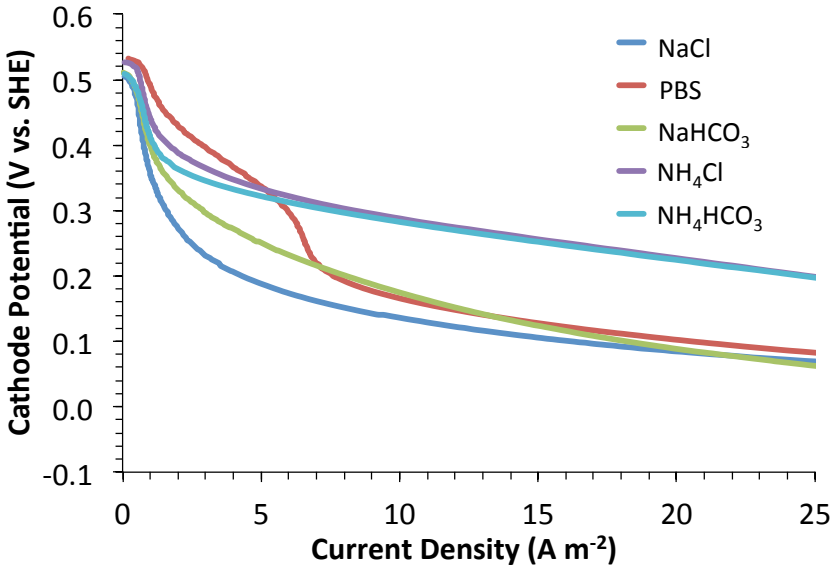

Figure 5.4. *Polarization curves of Pt-based gas-diffusion cathodes in different 50-mM solutions.*

The results in Figure 5.4 show that it is possible to save >150 mV at current densities >10 A m^{-2} using NH_4^+ as a buffer at the same concentrations as phosphate. This is an important result and has especially favorable implications for treatment of streams containing high levels of NH_4^+, such as animal waste. However, it has been shown in the past that NH_3 can be lost through air-cathodes in MFCs following deprotonation of NH_4^+. Thus, any NH_3 that partitions in the gas phase at the cathode should be recovered to sustainably use the buffer.

Next, we studied the importance of NH_4^+ transport on cathode performance; we obtained polarization curves for cathodes constructed with Nafion binder in solutions of different concentrations of NH_4^+. These results are shown in Figure 5.5. The experiments confirm that cathode performance was directly related to NH_4^+ concentration and, thus, its transport. Most notably, we saw the inflections in LSVs within the tested range of current densities that we observed earlier with 50-mM PBS, this time with 10- and 25-mM NH_4Cl. Beyond the current densities where the inflection was observed, the transport of NH_4^+ was slower than the production of OH^-, and, logically, the inflection appeared at a lower current density for 10-mM NH_4Cl than for 25-mM NH_4Cl. At higher concentrations, NH_4^+ transport was not limiting within the range of current densities tested. Therefore, we saw no inflection points for NH_4Cl ≥50 mM.

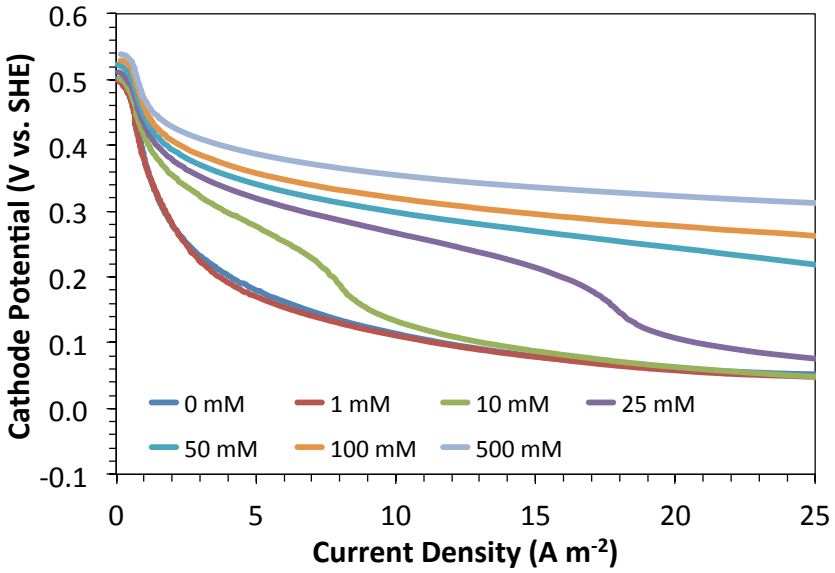

Figure 5.5. *Polarization curves of Pt-based gas-diffusion cathodes in solutions containing different concentrations (0-500 mM) NH_4Cl with 25-mM NaCl as background.*

6. Development of co-culture for enhanced energy recovery from sucrose:

One of our goals for this project was to achieve high current densities along with high Coulombic efficiencies when feeding sucrose as a substrate to MFCs. Since high current density producing ARB, such as *Geobacter* sp., can consume only simple substrates such as acetate, we developed a complementary mixed microbial culture that ferments sucrose primarily to acetate. We describe below our approach in developing such a homo-acetogenic culture, as well as its characterization in terms of electron recovery from sucrose as acetate and its community structure using molecular tools.

We set up a 0.5-L batch reactor fed with medium with the following composition (in 1 L): KH_2PO_4 0.2 g; NaCl 1 g; NH_4Cl 0.5 g; KCl 0.1 g; $MgCl_2 \bullet 6H_2O$ 0.25 g; $CaCl_2 \bullet 2H_2O$ 0.175 g; BES 6.02 g (for selective methanogenic inhibition), $NaHCO_3$ 4.2 g (50 mM); trace mineral media as published in Parameswaran et al (2009) 1mL; ATCC vitamins solution 0.5 mL, Fe^{2+} at 4 g/L 1 mL; and $Na_2S \bullet 7H_2O$ at 37 g/L 0.1 mL. We added 10 mmoles of sucrose to the batch reactor (i.e., 20 mM concentration). The initial medium pH was stable at around 6.75. We had previously enriched a consortium of homo-acetogenic bacteria from the suspension of an H-type MEC that produced current from a syntrophic interaction between homo-acetogens and ARB (Parameswaran et al, 2011). We added 5 mL of the enrichment culture to serve as inoculum

(1% of reactor volume) to obtain enrichment on sucrose, as well as conducting a thorough electron balance.

Batch reactions proceeded immediately, leading to complete sucrose utilization by the second day (Figure 6.1). The reactor pH dropped to 6.05 on day 2, but quickly stabilized back to 6.5 after that time point, and it remained stable until the end of batch operation (day 7). Of the characterized soluble products at the end of the batch run, lactate was the dominant sink, followed by acetate. Formate is a precursor for homo-acetogenesis (Ha et al, 2008) and should be considered as a readily utilizable substrate when homo-acetogenesis is not limiting. Lactate, acetate, and formate constituted about 40% of the total electrons from sucrose at the end of the batch run.

After a week of batch operation, we shifted the reactor to semi-continuous mode along with an increase in buffer concentration to 100 mM bicarbonate and a decrease in sucrose influent concentration to 10 mM. Semi-continuous operation involved replacing 200 mL of the medium once a week. Corresponding to this change, the product distribution shifted to almost all acetate (~75% of the total electrons), along with some propionate (7% of total electrons) and the rest as biomass (Figure 6.1), after 23 days of semi-continuous operation. The pH in the reactor remained steady at around 7.

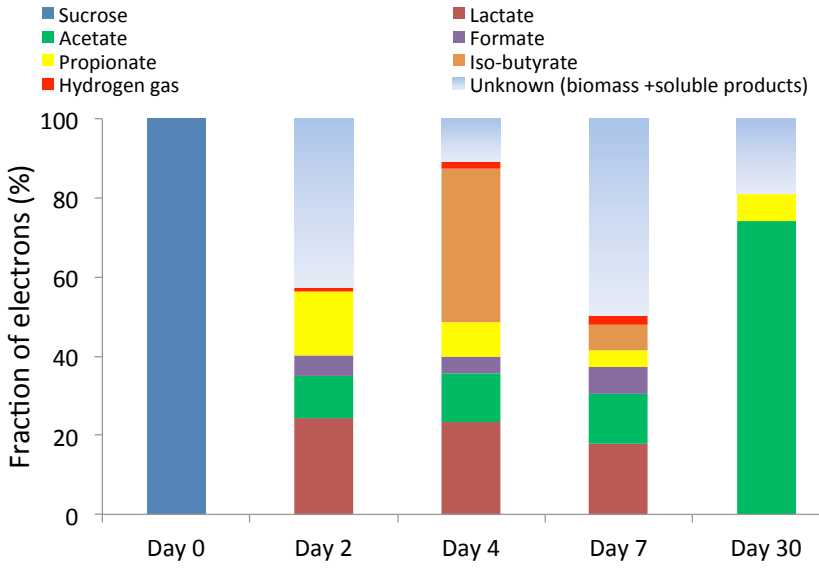

Figure 6.1. *Electron flow distribution during batch (up to day 7) and subsequent semi-continuous (day 30) operation of fermentation reaction fed with sucrose. The electron balance shifted from lactate, acetate, formate, and propionate during batch operation to predominantly acetate during semi-continuous operation.*

We obtained pellets from the suspension of the semi-continuous reactor after 2 months of steady-state operation. We extracted DNA from the pellets after freezing them overnight at -20 °C using RNeasy Blood and Tissue kit according to manufacturer's instructions along with modifications according to Ziv-El et al (2011). We quantified the extracted DNA using a Nanodrop spectrophotometer. We amplified the 16S rRNA gene for general bacteria using primers 8F and 1525R (Lane, 1991), after which the PCR products were purified for clone library preparation. We performed clone library analysis using TOPO TA cloning kit for sequencing, according to manufacturer's instructions. We sequenced the inserted PCR products and analyzed the closest match with BLAST software. A total of 63 clones were picked (Figure 6.2).

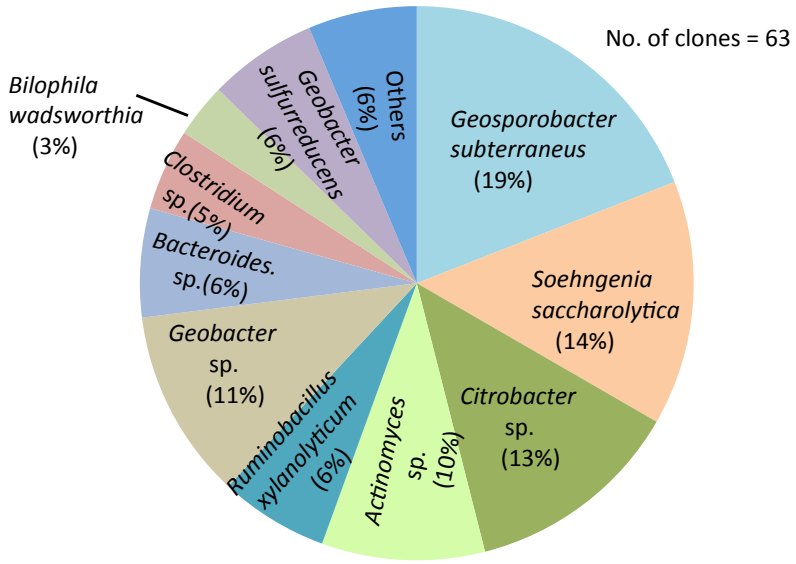

Figure 6.2. *Clone library analysis based on the 16S rRNA for the sucrose enrichment culture that converted sucrose predominantly to acetate and some propionate.*

The obligate anaerobic fermentative bacterium, *Geosporobacter subterraneus*, comprised around 19% of the total clones. *Geosporobacter* belongs to the *Clostridiales* order and it ferments sugars such as glucose and sucrose, to mainly acetate, H_2, and CO_2 with a growth optimum temperature of 42 °C and pH of 7.3 (Klouche et al, 2007). *Soehngenia saccharolytica*, belonging to cluster XII of *Clostridia*, accounted for 14% of the clones - it is anaerobic, aerotolerant, and saccharolytic, with major end products of sugar fermentation being acetate, formate, H_2, CO_2, and ethanol (Parshina et al, 2003). *Citrobacter amalonaticus* (13% of total clones) belongs to the *Enterobacteriaceae* family and is known to perform biological water gas shift reaction to produce hydrogen gas from carbon monoxide (Robaire, 2006) when supplemented with glucose/sucrose as carbon source.

Ruminobacillus xylanolyticum is another know genus of heterotrophic homo-acetogens that posses the capability to produce acetate either from sugars or from H_2/CO_2 (Drake HL, 1994). Since the enrichment was obtained from the suspension of an MEC anode, we also observed *Geobacter* sp. (11%) and *Geobacter sulfurreducens* (6%). However, their role towards sucrose fermentation is unclear. *Actinomyces* sp. (10% of total clones) and *Bacteroides* sp. (3%) are often associated with anaerobic biofilms such as MEC anodes. However, their role with respect to sucrose fermentation is also unknown.

To determine the possibility of achieving high Coulombic efficiencies from sucrose, the homo-acetogenic culture described above was combined with a highly enriched with *Geobacter* sp. in flat-plate MEC anodes producing high current densities (described in Section 4). We first acclimatized the acetate-fed ARB grown in the flat-plate MEC with 100 mM phosphate buffer solution to anaerobic media containing 100 mM $NaHCO_3$. After the medium change, a steady current density of 300 A/m^3_{anode} was sustained for a few days under continuous mode of operation, at which point we shifted to batch mode so as to starve the biofilm (Figure 6.3). When the current density dropped to around 10% of the maximum value (~ 30 A/m^3_{anode}), we replaced the anode content with the basal sucrose enrichment medium through continuous flow, but without sucrose addition (Figure 6.3).

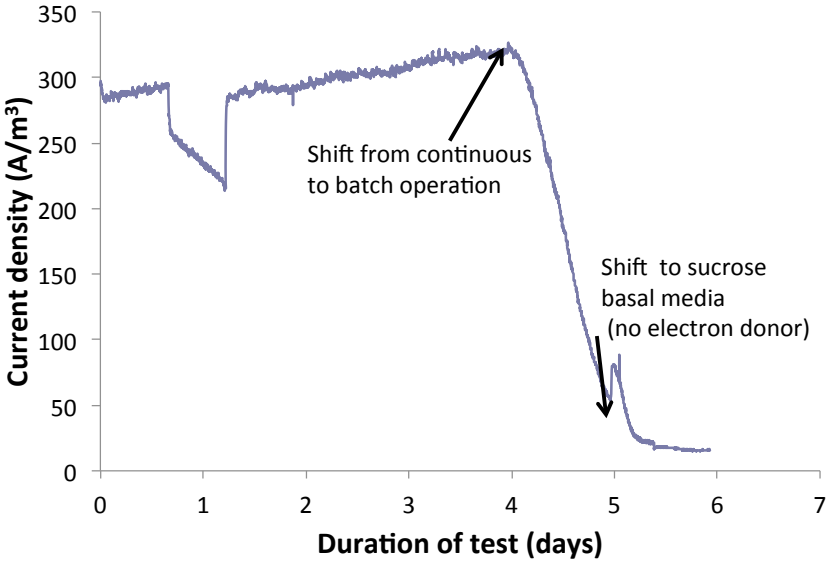

Figure 6.3*. Volumetric current density for the acetate-fed flat plate MEC before the electron-balance experiment with the sucrose co-culture.*

We started the electron balance experiment with the sucrose co-culture, after waiting for three HRTs (1 HRT = 9 hours) to ensure sufficient medium replacement. Then, we separately added a

pellet of the sucrose enrichment culture and 5 mM sucrose into the anode chamber. We obtained an initial sample from the MEC anode at time t = 0 for quantifying the exact amount of sucrose and other organic acids by high performance liquid chromatography (HPLC) equipped with BIORAD Aminex HPX-87H column for sugars and volatile acids analysis. Sucrose analysis employed water as the eluent phase, while the column was kept at 30 °C and a refractive index detector (RID) served as the detector. We analyzed volatile acids and alcohols using methods described in Parameswaran et al (2009).

Current density increased instantaneously to 27 A/m^3 after the spike, and then it increased rapidly over the next several hours to reach a maximum value of 150 A/m^3 (Figure 6.4). This is half the maximum current density under acetate-fed conditions. The maximum current density was sustained for about 6 hours, after which it rapidly declined to stabilize around 20 A/m^3. HPLC analysis indicated that the influent sucrose concentration was 5.6 (±0.02) mM, while no sucrose was detected at the end of the batch operation. We did not detect acetate or other volatile acids at the start or end of the batch run. Coulombic efficiency, based on sucrose removal, was 97% (Figure 6.4). Current from decaying biomass in the biofilm anode could be a significant fraction of the observed current density, as indicated by the tail end of Figure 6.4, which was still hovering around 20 A/m^3 for about 2 days. A conservative estimate of Coulombic efficiency after discarding all current density observed after 2.5 days still is 82%.

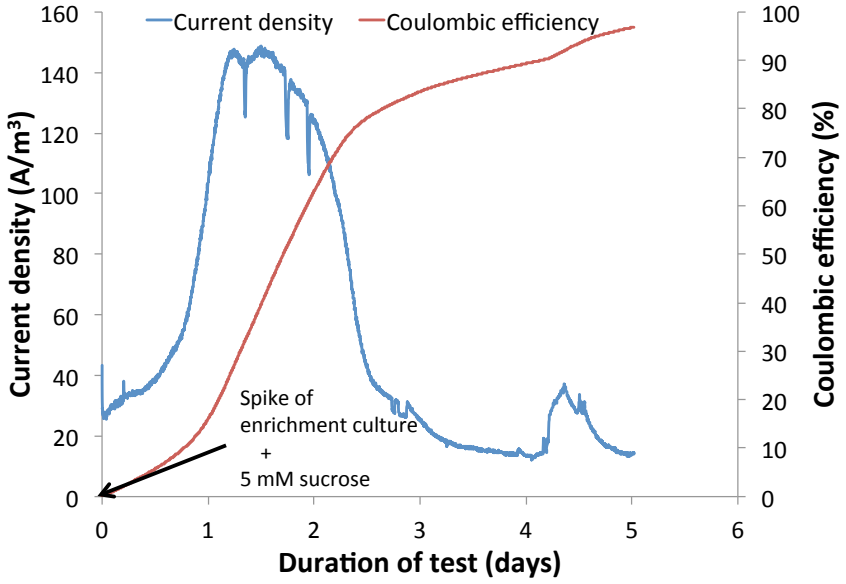

Figure 6.4. *Batch sucrose co-culture MEC operation indicating the observed current density and Coulombic efficiency.*

Recent research with sucrose- fed microbial fuel cells have shown Coulombic efficiencies ranging from 4% in single chamber MFCs (Beecroft et al., 2012) to a maximum of 92% in two-stage modular MFCs (Kim et al., 2010). Our results are a first documentation of very high Coulombic efficiency from sucrose during combined fermentation + anode respiration in a single-step MEC anode.

7. Summary and Conclusions

An MFC is a complex biological and electrochemical reactor in which different processes should be optimized in order to maximize current and power outputs. Throughout our project, we optimized materials, configurations, cathodic reactions, and microbial communities. The selection of anode materials proved to be an important parameter to optimize an MFC. Certain materials, such as stainless steel, reduce ARB performance and current production. On the other hand, the selection of an AEM that minimizes potential losses in an MFC yielded only a small improvement in the overall performance of the MFC. Our results show that most of the potential losses in an MFC occur at the cathode, where a pH gradient creates a concentration overpotential that can be responsible for the loss of up to ~30% of the energy available in an MFC. We provide a few strategies to minimize pH gradients and prevent potential losses.

Based on the analysis above, we built and tested a prototype MFC that produced up to 500 A/m_{anode}^3. An important characteristic of our MFC prototype is the short distance between anode and cathode (< 0.5 cm). Based on our calculations, this short distance is required to achieve high power densities in an MFC. Longer distances between anode and cathode result in prohibitively large Ohmic losses that reduce the operating potential of the MFC.

Finally, we optimized a microbial community for the consumption of sucrose, achieving a Coulombic efficiency of > 90%. Our experiments show the importance of optimizing microbial communities in MFCs in order to maximize electron recoveries. Combining our individual results, we have made significant progress towards the development of an efficient sucrose-fed microbial fuel cell.

References

- Beecroft NJ, Zhao F, Varcoe JR, Slade RCT, Thumser AE, Avignone-Rossa C. 2012. Dynamic changes in microbial community composition in microbial fuel cells fed with sucrose. Appl Microbiol Biotechnol 93: 423-437.
- Chaudhuri SK, Lovley DR. 2003. Electricity generation by direct oxidation of glucose in mediatorless microbial fuel cells. Nat Biotechnol 21(10): 1229-1232.
- Cheng S, Liu H, Logan BE. 2006. Increased performance of single-chamber microbial fuel cells using an improved cathode structure. Electrochem Comm 8:489-494.
- Drake HL. 1994. Acetogenesis. In Chapman and Hall Microbiology Series. London: Chapman Hall.
- Dumas C, Basseguy R, Bergel A. 2008. DSA to grow electrochemically active biofilms of *Geobacter sulfurreducens*. Electrochim Acta 53(7):3200-3209.
- Fan YZ, Hu HQ, Liu H. 2007. Sustainable power generation in microbial fuel cells using bicarbonate buffer and proton transfer mechanisms. Environ Sci Technol 42(23): 8154-8158.
- Fang J, Shen PK. 2006. Quaternized poly(phthalazinon ether sulfone ketone) membrane for anion exchange membrane fuel cells. J Membrane Sci 285(1-2): 317-322.
- Ha PT, Tae B, Chang IS. 2008. Performance and bacterial consortium of microbial fuel cell fed with formate. Energy & Fuels 22(1):164-168.
- He Z, Wagner N, Minteer SD, Angenent LT. 2006. An Upflow Microbial Fuel Cell with an Interior Cathode: Assessment of the Internal Resistance by Impedance Spectroscopy. Environ Sci Technol 40: 5212-5217.
- Inoue K, Leang C, Franks AE, Woodard TL, Nevin KP, Lovley DR. 2011. Specific localization of the c-type cytochrome OmcZ at the anode surface in current-producing biofilms of *Geobacter sulfurreducens*. Environ Microbiol Reports 3(2): 211-217.
- Kim JR, Oh SE, Cheng S, Logan BE. 2007. Power generation using different cation, anion and ultrafiltration membranes in microbial fuel cells. Environ Sci Technol 41(3): 1004-1009.
- Kim JR, Premier GC, Hawkes FR, Rodriguez J, Dinsdale RM, Guwy AJ. 2010. Modular tubular microbial fuel cells for energy recovery during sucrose wastewater treatment at low organic loading rate. 101: 1190-1198.
- Klouche N, Fardea ML, Lascourrèga JF, Cayo JL, Hacen H, Thomas P, Magot M. 2007. *Geosporobacter subterraneus* sp. nov., a spore forming bacterium isolated from a deep subsurface aquifer. Int J Syst Evol Microbiol 57: 1757-1761.
- Lane DJ. 1991. 16S/23S rRNA sequencing. In: Stackebrandt, E., Goodfellow, M. (Eds), Modern microbiological methods. Wiley, Chichester, New York, pp: 115-175.
- Lee HS, Rittmann BE. 2010. Significance of Biological Hydrogen Oxidation in a Continuous Single-Chamber Microbial Electrolysis Cell. Environ Sci Technol 44: 948-954.
- Liu H, Cheng SA, Logan BE. 2005. Production of electricity from acetate or butyrate using a single-chamber microbial fuel cell. Environ Sci Technol 39(2): 658-662.

- Logan BE, Hamelers B, Rozendal RA, Schröder U, Keller J, Freguia S, Aelterman P, Verstraete W, Rabaey K. 2006. Microbial fuel cells: Methodology and technology. Environ Sci Technol 40:5181–5192.
- Logan BE, Cheng S, Watson V, Estadt G. 2007. Graphite Fiber Brush Anodes for Increased Power Production in Air-Cathode Microbial Fuel Cells. Environ Sci Technol 41(9):3341-3346.
- Marcus AK, Torres CI, Rittmann BE. 2007. Conduction-based modeling of the biofilm anode of a microbial fuel cell. Biotechnol Bioeng 98(6):1171-1182.
- Parameswaran P, Torres CI, Lee HS, Krajmalnik-Brown R, Rittmann BE. 2009. Syntrophic interactions between anode-respiring bacteria (ARB) and non-ARB in a biofilm anode: electron balances. Biotech Bioeng 103(3): 513-523.
- Parameswaran P, Torres CI, Lee HS, Rittmann BE, Krajmalnik-Brown R. 2011. Hydrogen consumption in microbial electrochemical systems (MXCs): The role of homo-acetogenic bacteria. Bioresource Technol 102(1): 263-271.
- Parshina SN, Kleerebezem R, Sanz JL, Letting G, Nozhevnikova AN, Kostrikina NA, Lysenko AM, Stams AJM. 2003. *Soehngenia saccharolytica* sp. nov. and *Clostridium amygdalinum* sp. nov., two novel anaerobic benzaldehyde-converting bacteria. Int J Syst Evol Microbiol 53: 1791-1799.
- Perlack RD, Wright LL, et al. 2005. Biomass as Feedstock for a bioenergy and bioproducts industry: the technical feasibility of a billion-ton annual supply. U.S. DOE/USDA report.
- Piela P, Wrona PK. 2006. Some anion-transport properties of Nafion (TM) 117 from fuel cell hydrogen peroxide generation data. J Power Sources 158(2): 1262-1269.
- Richter H, McKarthy K, Nevin KP, Johnson JP, Rotello VM, Lovley DR. 2008. Electricity generation by Geobacter sulfurreducens attached to gold electrodes. Langmuir 24: 4376- 4379.
- Rismani-Yazdi H, Carver SM, Christy AD, Tuovinen IH. 2008. Cathodic limitations in microbial fuel cells: An overview. J Power Sources 180(2): 683-694.
- Robaire, S. Master's thesis, 2006. Biological hydrogen production using *Citrobacter amalonaticus* Y19 to catalyze the water gas shift reaction. The University of British Columbia
- Rozendal RA, Hamelers HVM, Molenkmp RJ, Buisman CJN. 2007. Performance of single chamber biocatalyzed electrolysis with different types of ion exchange membranes. Water Res 41: 1984-1994.
- Rozendal RA, Hamelers HVM, Rabaey K, Keller J, Buisman CJN. 2008. Towards practical implementation of bioelectrochemical wastewater treatment. Trends Biotechnol 26(8): 450-459.
- Sleutels THJA, Hamelers HVM, Rozendal RA, Buisman CJN. 2009. Ion transport resistance in Microbial Electrolysis Cells with anion and cation exchange membranes. Int J Hydrogen Energy 34(9): 3612-3620.
- Ter Heijne A, Hamelers HVM, De Wilde V, Rozendal RA, Buisman CJN. 2006. A bipolar membrane combined with ferric iron reduction as an efficient cathode system in microbial fuel cells. Environ Sci Technol 40:5200-5205.
- Torres CI, Marcus AK, Rittmann BE. 2007. Kinetics of Consumption of Fermentation Products by Anode-Respiring Bacteria. Appl Microbiol Biot 77(3): 689-697.

- Torres CI, Marcus AK, Parameswaran P, Rittmann BE. 2008a. Kinetic experiments for evaluating the Nernst-Monod model for anode-respiring bacteria (ARB) in a biofilm anode. Environ Sci Technol 42(17): 6593-6597.
- Torres CI, Marcus AK, Rittmann BE. 2008b. Proton transport inside the biofilm limits electrical current generation by anode-respiring bacteria. Biotechnol Bioeng. 100(5): 872-881.
- Torres CI, Lee HS, Rittmann BE. 2008c. Carbonate species as OH- carriers for decreasing the pH gradient between cathode and anode in biofuel-cells. Environ Sci Technol 42(23): 8773- 8777.
- Torres CI, Krajmalnik-Brown R, Parameswaran P, Marcus AK, Wanger G, Gorby YA, Rittmann BE. 2009. Selecting anode-respiring bacteria based on anode potential: Phylogenetic, electrochemical and microscopic characterization. Environ Sci Technol 43(24): 9519-9524.
- U.S. Department of Energy, Office of the Biomass Program. 2009. Multiyear Program Plan 2007-2017.
- Varcoe JR, Slade RCT. 2005. Prospects for alkaline anion-exchange membranes in low temperature fuel cells. Fuel Cells 5(2): 187-200.
- Varcoe JR, Slade RCT, Lam How Yee E. 2006. An alkaline polymer electrochemical interface: a breakthrough in application of alkaline anion-exchange membranes in fuel cells. Chem Comm 13:1428-1429.
- Warner J, Singer PW. 2009. Fueling the Balance: A Defense Energy Strategy Primer, Foreign Policy at Brookings.
- Xiong Y, Fang J, Zeng QH. Liu QL. 2008. Preparation and characterization of cross-linked quaternized poly(vinyl alcohol) membranes for anion exchange membrane fuel cells. J Membrane Sci 311(1-2): 319-325.
- Zhang F, Merrill MD, Tokash JC, Saito T, Cheng S, Hickner MA, Logan BE. 2011. Mesh optimization for microbial fuel cell cathodes constructed around stainless steel mesh current collectors. J Power Sources. 196(3):1097–1102.
- Zhang X, Cheng S, Huang X, Logan BE. 2010. Improved performance of single-chamber microbial fuel cells through control of membrane deformation. Biosen Bioelectron 25(7):1553-1858.
- Zhao F, Harnisch F, Schroeder U, Scholz F, Bogdanoff P, Herrmann I. 2006. Challenges and constraints of using oxygen cathodes in microbial fuel cells. Environ Sci Technol 40(17): 5193-5199.
- Ziv-El M, Delgado AG, Yao Y, Kang DW, Nelson KG, Halden RU, Krajmalnik-Brown R. 2011. Development and characterization of DehaloR^2, a novel anaerobic microbial consortium performing rapid dechlorination to ethene. Appl Microbiol Biotechnol 92: 1063-1071.

DOI: 10.1002/cssc.201100777

Importance of OH^- Transport from Cathodes in Microbial Fuel Cells

Sudeep C. Popat, Dongwon Ki, Bruce E. Rittmann, and César I. Torres*[a]

Cathodic limitation in microbial fuel cells (MFCs) is considered an important hurdle towards practical application as a bioenergy technology. The oxygen reduction reaction (ORR) needs to occur in MFCs under significantly different conditions compared to chemical fuel cells, including a neutral pH. The common reason cited for cathodic limitation is the difficulty in providing protons to the catalyst sites. Here, we show that it is not the availability of protons, but the transport of OH^- from the catalyst layer to the bulk liquid that largely governs cathodic potential losses. OH^- is a product of an ORR mechanism that has not been considered dominant before. The accumulation of OH^- at the catalyst sites results in an increase in the local cathode pH, resulting in Nernstian concentration losses. For Pt-based gas-diffusion cathodes, using polarization curves developed in unbuffered and buffered solutions, we quantified this loss to be >0.3 V at a current density of 10 $A\,m^{-2}$. We show that this loss can be partially overcome by replacing the Nafion binder used in the cathode catalyst layer with an anion-conducting binder and by providing additional buffer to the cathode catalyst directly in the form of CO_2, which results in enhanced OH^- transport. Our results provide a comprehensive analysis of cathodic limitations in MFCs and should allow researchers to develop and select materials for the construction of MFC cathodes and identify operational conditions that will help minimize Nernstian concentration losses due to pH gradients.

Introduction

Microbial fuel cells (MFCs) are devices in which anode-respiring bacteria (ARB) oxidize organic compounds and transfer electrons to an electrode.[1] These electrons move through a circuit to a cathode, where oxygen is reduced, usually on a metal catalyst, although biological entities, including microorganisms and enzymes, can also be used as catalysts.[1] MFCs provide a tremendous opportunity to achieve sustainable wastewater treatment as it is possible to recover energy from the organics present in wastewater directly as electrical power.[1a,2] The maximum available voltage in an MFC is approximately 1.1 V, on the basis of the redox potential for the oxidation of acetate, a commonly used electron donor, and the complete reduction of O_2 to water or OH^-, both at pH 7.[1b] Note that near-neutral pH is required for the optimum growth and activity of ARB at the anode.[3]

Cell voltages obtained with appreciable current densities are typically less than 0.5 V, resulting in poor voltage efficiency and low power densities.[2c,4] Kinetic studies of ARB have revealed that maximum current densities ($\approx$10 $A\,m^{-2}$) can be achieved with anodic potential losses of only 0.1–0.2 V.[5] More recently, current densities of up to 30 $A\,m^{-2}$ have been achieved with similar potential losses when using 3D anodes.[6] On the other hand, cathodic potential losses at these current densities, when using metal catalysts, have been shown to be >0.5 V.[2c,7] This clearly underscores the need to improve cathode performance to make MFCs more efficient. In this study, we aimed to elucidate the crucial factors that lead to cathodic limitation in MFCs. We focus primarily on cathodes based on metal catalysts as current densities achieved with biological catalysts are yet too low for any practical application.

The typical 4 e^- oxygen reduction reaction (ORR) proceeds on metal catalysts through either of the following two mechanisms, depending on the reaction conditions [Eqs. (1) and (2)]:

$$O_2 + 4\,e^- + 4\,H^+ \rightarrow 2\,H_2O \quad (1)$$

$$O_2 + 4\,e^- + 2\,H_2O \rightarrow 4\,OH^- \quad (2)$$

A common perception among researchers working on MFCs is that the ORR proceeds through the mechanism shown in Equation (1) as is the case for cathodes in proton exchange membrane (PEM) fuel cells.[1a,b,2c] However, cathodes in MFCs are subjected to significantly different conditions than in PEM fuel cells, for example, direct contact with an electrolyte at neutral pH. Thus, we first analyze whether this minimal availability of protons as reactant can support the cathodic current densities typically observed in MFCs. We use the case of gas-diffusion cathodes throughout this study as these are the most popular and practically feasible form of cathodes currently developed.

We show in Scheme 1 a a schematic of the cathode structure in MFCs as it is used in single-chamber MFCs. This includes

[a] Dr. S. C. Popat, D. Ki, Dr. B. E. Rittmann, Dr. C. I. Torres
Swette Center for Environmental Biotechnology, Biodesign Institute
Arizona State University
727 E Tyler St, Tempe, AZ 85287 (USA)
Fax: (+1) 480-727-0889
E-mail: cit@asu.edu

Supporting Information for this article is available on the WWW under http://dx.doi.org/10.1002/cssc.201100777.

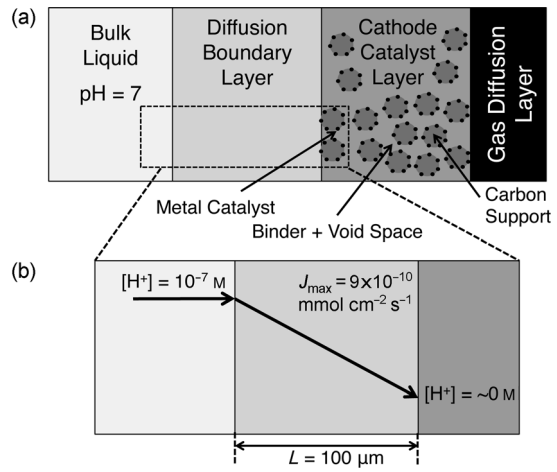

Scheme 1. (a) Schematic of the cathode structure in MFCs. (b) Hypothetical case of proton transport through the diffusion boundary layer. The flux of protons was determined using Fick's first law of diffusion with a diffusion coefficient of protons $= 9\times10^{-5}$ cm^2 s^{-1}.[8]

a gas diffusion layer to allow efficient O_2 transport to the active catalyst sites, the cathode catalyst layer that is comprised of the metal catalyst (usually supported on carbon) and an ion-conducting catalyst binder to create a three-phase boundary required for the ORR, and a diffusion boundary layer at the interface with the bulk liquid. If the ORR proceeds on cathodes in MFCs through the mechanism shown in Equation (1), the flux of protons through the catalyst layer and the diffusion boundary layer has to be sufficient to support the current densities of 5–10 A m^{-2} that are usually observed. This transport of protons occurs mainly through diffusion, according to Fick's law [Eq. (3)]:

$$J_{H^+} = \frac{D_{H^+}\left(C^0_{H^+} - C^*_{H^+}\right)}{L} \quad (3)$$

where J_{H+} is the rate of transport of protons from the bulk liquid to the catalyst sites [mmol cm^{-2} s^{-1}], C^0_{H+} and C^*_{H+} are the bulk liquid and the local cathode concentrations of protons, respectively [mmol cm^{-3}], D_{H+} is the cumulative diffusion coefficient of protons in the combined catalyst and diffusion boundary layers [cm^2 s^{-1}], and L is the entire length of diffusion [cm].

The maximum concentration gradient that can exist for the transport of protons through the diffusion boundary layer, when the bulk liquid is at pH 7, is approximately 10^{-7} M (Scheme 1 b). We need to assume a thickness L for the diffusion boundary layer to determine the flux of protons through it. This thickness depends on the hydrodynamic conditions at the interface, and the smallest value is tens of microns for well-stirred solutions.[9] However, MFCs are typically unstirred or mildly stirred; thus, this diffusion boundary layer can easily be >100 μm thick.[9] Assuming a 100 μm thick diffusion boundary layer, we determined that the maximum flux of protons through it will be approximately 9×10^{-10} mmol cm^{-2} s^{-1}. This corresponds to a maximum current density of only approximately 8.5×10^{-3} A m^{-2}, which is about three orders of magnitude lower than the typically observed current densities in MFCs. This analysis does not include the resistance to proton transport in the cathode catalyst layer, which will further reduce the actual flux to the active catalyst sites. Thus, we conclude that the ORR cannot proceed on cathodes in MFCs through the mechanism shown in Equation (1); it must occur through the mechanism shown in Equation (2), as it does in alkaline fuel cells.[10] Other authors have already suggested that the ORR, in electrolytes with a neutral to alkaline pH, proceeds through the latter mechanism, irrespective of the metal catalyst used.[11] Note that our analysis here applies not just to gas-diffusion cathodes in single-chamber MFCs, but to any cathode containing a metal catalyst that is bound onto a support (e.g., carbon cloth) with a polymeric binder and/or surrounded by bulk electrolyte, either liquid or membrane, at neutral pH.

An important implication of the mechanism shown in Equation (2) is that it is OH^- transport, not proton transport, that governs cathode performance in MFCs. An inability to rapidly transport OH^- from the active catalyst sites to the bulk liquid will result in an increase in its local concentration, leading to concentration overpotential (η_{conc}). Cathodic η_{conc} in chemical fuel cells is often associated with mass transport limitations of O_2 (a reactant) at high current densities.[12] As we will explain in the next section, η_{conc} in MFCs can occur even at low current densities as a result of Nernstian losses due to an increase in the local concentration of OH^- (a product) and, hence, local cathode pH value. From the Nernst equation, every increase in one pH unit decreases the redox potential for the ORR by approximately 59 mV (at room temperature).[1b] We hypothesize that this Nernstian η_{conc}, a result of poor OH^- transport (referred to from hereon as $\eta_{[OH^-]}$), could contribute significantly to the cathodic potential losses typically observed in MFCs.

We show in Scheme 2 that resistances to OH^- transport exist in the cathode catalyst layer and the diffusion boundary layer. The flux of OH^- through each layer depends on the diffusion coefficients of OH^- in each (D_{OH^-}), as well as the thickness of each (L). To transport OH^- from the active catalyst sites to the bulk liquid, the presence of an OH^- concentration gradient is necessary. However, to minimize $\eta_{[OH^-]}$, we must also minimize the OH^- concentration gradient. Therefore, it is essential

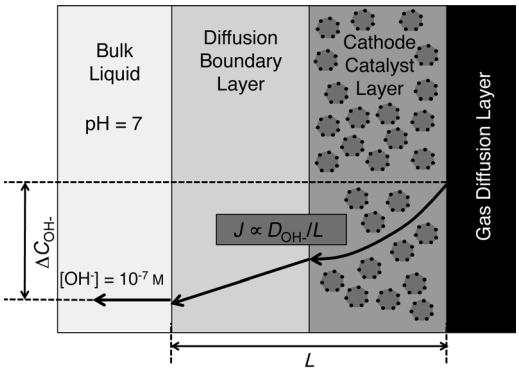

Scheme 2. Schematic of OH^- transport from the cathode catalyst layer to the bulk liquid. D_{OH^-} and L are represented as cumulative parameters for the diffusion boundary layer and the cathode catalyst layer together.

to have a very large D_{OH^-}/L, so that a high flux of OH^- can be maintained with smaller concentration gradients; this leads to a lower local pH value for a specific current density (or rate of OH^- production). $\eta_{[OH^-]}$ is important in MFC cathodes because the bulk liquid has a very low concentration of OH^- ($\approx 10^{-7}$ M), and even low current densities and concentration gradients will lead to significant losses. In contrast, alkaline fuel cells have an electrolyte at pH 14 ($[OH^-] = 1$ M); even at modest current densities and concentration gradients, the pH increase is negligible, thus making $\eta_{[OH^-]}$ unimportant. The same holds true also for $\eta_{[H^+]}$ (i.e., the Nernstian concentration overpotential related to lower local proton concentration) in PEM fuel cells, where consumption of protons at moderate current densities hardly changes the local cathode pH value.

Potential losses based on the pH value are often acknowledged in MFCs when a membrane is used to separate the anode and the cathode chambers.[13] These occur because cations other than protons (the product of anode respiration) are transported from the anode to the cathode through the cation exchange membrane typically used. The transport of other cations (instead of protons) results in a decrease in the pH value of the anode chamber and an increase in the pH value of the cathode chamber.[14] A common approach taken to avoid these losses is to exclude the membrane.[1c] However, we stress here that pH-based losses associated with the cathode could occur even in the absence of the membrane because of OH^- transport limitation in the cathode catalyst and diffusion boundary layers.

Based on OH^- transport, we argue that current MFC designs lead to a considerable $\eta_{[OH^-]}$ in cathodes. The first reason stems from the anion-conducting properties of the catalyst binder used for creating a three-phase boundary for the ORR. As an extrapolation from its use in PEM fuel cells, Nafion has been the binder of choice in cathodes in MFCs.[15] However, Nafion contains sulfonate moieties that are efficient in transporting cations, but provide significant resistance to the transport of anions.[16] Using Nafion as the binder in cathodes in MFCs should thus lead to small D_{OH^-}/L values for the cathode catalyst layer, which would result in a high local concentration of OH^- and high local cathode pH value. Recent studies have shown that increasing the sulfonation of the binders used in cathodes in MFCs results in poorer performance, whereas replacing Nafion with a polymer that lacks sulfonate moieties or excluding the binder altogether results in lower cathodic potential losses, indirectly corroborating our hypothesis here.[17] The second reason is the lack of sufficient agitation, which results in a significant diffusion boundary layer, as we mentioned earlier. Decreasing the diffusion boundary layer thickness would require increasing the agitation rates, which presents a challenge for the practical application of additional electrical energy input.

We note that buffers used in MFCs could aid in OH^- transport through the cathode catalyst and diffusion boundary layers. For example, when phosphate is used as a buffer, the $H_2PO_4^-$ species can deprotonate to HPO_4^{2-}, which acts as an OH^- carrier. However, the diffusion coefficients of carriers such as HPO_4^{2-} in water are an order of magnitude lower than that of OH^-.[18] In addition, Nafion provides significant resistance to transport of these anions in the cathode catalyst layer. An increase in local pH would rapidly lead to unfavorable concentration gradients for the relevant buffer species. Thus, we anticipate that buffers will be able to aid in OH^- transport only in a certain range of current densities, which is as yet undetermined.

In this study, we aimed to determine the magnitude of $\eta_{[OH^-]}$ as a result of the increase in the local OH^- concentration in MFC cathodes by using gas-diffusion cathodes as they are used in single-chamber MFCs as an example. We used polarization curves developed for cathodes under various conditions in gas-diffusion half cells to show that these losses are significant and can explain the poor cathode performance in MFCs compared to chemical fuel cells. We also show that phosphate buffer helps decrease $\eta_{[OH^-]}$ only at low current densities; higher current densities make it impossible to maintain a neutral local cathode pH value. We also show that these losses can be mitigated to some extent by replacing Nafion as the catalyst binder with an anion-conducting polymer, which results in significantly larger D/L values for OH^- and the anionic buffers. Finally, we show that providing an additional OH^- carrier to the cathode in the form of CO_2, which is fed in a mixture with air, further improves cathode performance by reducing the local cathode pH value and, thus, $\eta_{[OH^-]}$.

Overview of potential losses

We describe here some fundamentals of electrochemical reaction kinetics and associated potential losses that we use to elucidate the importance of OH^- transport in cathodes in MFCs.[19] For all electrochemical reactions occurring on an electrode surrounded by an electrolyte, two types of potential losses occur under polarized conditions. The first is the activation loss (η_{act}), which is associated with the potential barrier of the reaction. The relationship between electrical current density (j) and η_{act} is described by the Butler–Volmer equation [Eq. (4)], which is shown here for ORR:

$$j = j_0\left(\frac{C^*_{O_2}}{C^{0*}_{O_2}} e^{\frac{\alpha n F \eta_{act}}{RT}} - \frac{C^*_{OH^-}}{C^{0*}_{OH^-}} e^{\frac{-(1-\alpha) n F \eta_{act}}{RT}}\right) \quad (4)$$

where j_0, α, and n are the exchange current density [A m^{-2}], charge transfer coefficient, and the number of electrons transferred, respectively, which are properties of the catalyst used for the ORR (Pt in our experiments). Briefly, j_0 is the background current density at zero net overpotential, and α is the fraction of the thermodynamic potential available at the electrode–electrolyte interface that helps to lower the activation energy. C^* denotes the actual concentrations at the catalyst surface, whereas C^{0*} stands for reference concentrations. Note that the term associated with the product (OH^-) concentrations in Equation (4) becomes negligible with increasing η_{act}. As we will show later, this is the case for ORR on Pt at current densities typically observed in MFCs. Consequently, we use the Butler–Volmer equation in this simpler form [Eq. (5)]:

$$j = j_0\left(\frac{C^*_{O_2}}{C^{0*}_{O_2}} e^{\frac{\alpha n F \eta_{act}}{RT}}\right) \quad (5)$$

Equation (5) should describe cathode polarization curves as long as the only potential loss occurring is due to the activation barrier. Deviation from this equation indicates a second potential loss associated with the concentrations of the reactants and products (η_{conc}). The concentration of O_2, which is a reactant for the ORR, results in overpotentials in two ways. The first way occurs via directly affecting the kinetics described by the Butler–Volmer equation, where a decrease in $C^*_{O_2}$ decreases the electrical current. The second results from an effect on the reversible thermodynamic voltage described by the Nernst equation. We assume that concentration overpotentials related to O_2 are negligible in MFC cathodes as these typically occur at very high current densities that are not yet achieved in MFCs.[12,20]

Any deviations in cathode polarization curves from those calculated by using Equation (5) must be due to concentration losses associated with the product (OH^-, $\eta_{[OH^-]}$). OH^- concentrations affect the reversible thermodynamic voltage according to Equation (6):

$$\begin{aligned}\eta_{[OH^-]} &= E^0_{O_2/OH^-} - E^*_{O_2/OH^-} \\ &= \left[E^0 - \frac{RT}{nF}\ln\left(C^0_{OH^-}\right)\right] - \left[E^0 - \frac{RT}{nF}\ln\left(C^*_{OH^-}\right)\right] \\ &= \frac{RT}{nF}\ln\left(\frac{C^*_{OH^-}}{C^0_{OH^-}}\right)\end{aligned} \quad (6)$$

It is evident from Equation (6) that an increase in the local concentration of OH^- ($C^*_{OH^-}$) leads to an increased $\eta_{[OH^-]}$. $C^*_{OH^-}$ is directly related to the rate of transport of OH^- from the catalyst to the bulk liquid (J) through Fick's law, which for OH^- transport can be written as:

$$J = \frac{D_{OH^-}\left(C^*_{OH^-} - C^0_{OH^-}\right)}{L} \quad (7)$$

In this study, we use the above concepts to determine $C^*_{OH^-}$ and D_{OH^-}/L for cathodes in MFCs using polarization curves obtained in unbuffered solutions. We also extend our analysis to cathode performance in phosphate buffer, for which we determine $\eta_{[OH^-]}$.

Results and Discussion

Cathode performance in unbuffered solution

We first used linear sweep voltammetry (LSV) to obtain polarization curves for Pt-based gas-diffusion cathodes constructed with Nafion binder in unbuffered 100 mM $NaClO_4$ solution at pH 7.5, 10.8, or 13. The curves are shown in Figure 1. We obtained at least three polarization curves for each condition and show one representative set here. We provide an additional representative set in the Supporting Information as Figure S1. All replicate curves followed the same trend as shown here.

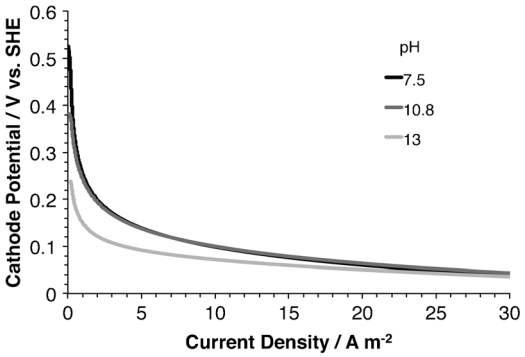

Figure 1. Polarization curves of Pt-based gas-diffusion cathodes constructed with Nafion binder in 100 mM $NaClO_4$ solution at different pH values.

As we have already mentioned, activation losses should not be different among the different conditions we tested, per Equation (5).

It is evident from Figure 1 that the cathode in pH 7.5 solution had the largest potential losses, particularly at low current densities. The cathode in pH 7.5 solution had the highest open circuit potential (OCP), a result of the lower initial pH value. Even so, the OCP was lower than the thermodynamic equilibrium potential of 0.78 V versus SHE (at pH 7.5), as expected for the $4e^-$ ORR. This loss on OCP (η_{mixed}) can be attributed to mixed potential caused by the competing $2e^-$ ORR that produces H_2O_2 (or HO_2^-) and has a thermodynamic equilibrium potential of 0.26 V versus SHE (at pH 7.5).[21]

The difference in potential for the cathode in pH 7.5 solution versus the cathodes in higher pH solutions was only maintained at current densities $< 1\ A\,m^{-2}$, indicative of high potential losses at low current densities. These losses also decreased with an increasing bulk liquid pH value, indicating that they are related directly to the concentration gradient for OH^- between the bulk liquid and the cathode. An effect of O_2 concentration on these losses can be ruled out as these current densities are well below what would cause losses due to O_2 limitation. Also, any losses due to O_2 limitation would not be a function of the bulk liquid pH value.

Eventually, all cathodes converged to the same potential at high current densities. η_{act} should be similar among the different conditions we tested here, per Equation (5), as it is related to the intrinsic properties of the catalyst used (Pt). η_{mixed} should also be similar. Therefore, the convergence of the cathode potentials suggests that they all reach the same local pH, irrespective of the bulk liquid pH value. This experiment thus provides the first indication of the importance of OH^- transport from cathodes and its resulting impact on $\eta_{[OH^-]}$.

We assume that $\eta_{[OH^-]}$ for the cathode in pH 13 solution should be negligible because, at the current densities tested, the local concentration of OH^- is not likely to increase by more than a few times the bulk liquid OH^- concentration; thus $\eta_{[OH^-]}$, if nonzero, would have been only a few tens of mV, compared to the other two conditions, for which it was likely to be hundreds of mV. We thus used the polarization curve for the cathode in pH 13 solution to determine the parameters related to catalyst activity, that is, j_0 and α.

At large values of η_{act}, the Butler–Volmer equation simplifies to the Tafel equation [Eq. (8)]:

$$\ln j = \ln j_0 + \frac{\alpha n F \eta_{act}}{RT} \quad (8)$$

to which the polarization curve can be fitted after including η_{mixed}. We obtained j_0 and α values of 9.5×10^{-8} A cm^{-2} and 0.195, respectively, as the averages from fitting the three polarization curves in pH 13 solution to the Tafel equation (Figure S2). These values are within the ranges that are typically observed for Pt for the 4 e$^-$ ORR.[22] Using the obtained values from the Tafel plot, the Butler–Volmer equation predicts the potential losses of the cathode in pH 13 solution (Figure S3).

Next, we used the j_0 and α values to predict the η_{act}-controlled response (including η_{mixed}) of the cathode in pH 7.5 solution using Equation (5) (shown in Figure 2). The actual response of the cathode was controlled by an additional overpotential, which should be $\eta_{[OH^-]}$. We thus performed further analyses to determine the transport properties of OH^- and the resulting local pH that would correspond to the $\eta_{[OH^-]}$ observed. The total potential loss for the cathode can be represented as Equation (9):

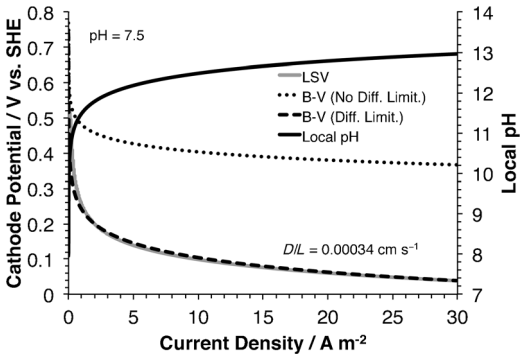

Figure 2. Comparison of polarization curve of Pt-based gas-diffusion cathode constructed with Nafion binder in 100 mM $NaClO_4$ solution at pH 7.5 with curves predicted from the Butler–Volmer equation without and with OH^- diffusion limitation, and the predicted local cathode pH value as a function of current density resulting from OH^- diffusion limitation.

$$\eta_{total} = \eta_{act} + \eta_{mixed} + \eta_{[OH^-]} \quad (9)$$

By using Equations (5), (6), and (9), the local concentration of OH^- could be obtained as a function of η_{total}, and thus the local cathode pH value could be determined. We show the local cathode pH value as a function of the current density in Figure 2. The pH value increased to >11 very rapidly at current densities <1 A m^{-2} and was >12.5 at 10 A m^{-2}. We fitted the local concentration of OH^- to Equation (7) to determine the cumulative D_{OH^-}/L value for OH^- transport through the cathode catalyst layer and diffusion boundary layer. A good fit was observed for a D_{OH^-}/L value of 0.00034 cm s^{-1} (Figure 2). If we assume that D_{OH^-} in Nafion is similar to that in water, this D_{OH^-}/L value corresponds to a diffusion length of around 1.550 mm. This length seems unreasonable, confirming that a large transport resistance exists in the cathode catalyst layer due to low D_{OH^-} in Nafion. Hence, the cathode catalyst layer caused a significant $\eta_{[OH^-]}$. The D_{OH^-}/L value determined here also fits the polarization curve for the cathode in pH 10.8 solution (Figure S4).

At 10 A m^{-2}, the η_{act} and η_{mixed} combined values are around 0.35 V (Figure 2), calculated by using Equation (5), which is the loss from the thermodynamic equilibrium potential of the ORR (0.78 V vs. SHE at pH 7.5) to the calculated Butler–Volmer curve. $\eta_{[OH^-]}$ is approximately 0.35 V, calculated as the difference between the Butler–Volmer calculation and the actual data obtained. This analysis shows that a significant fraction ($\approx$50%) of the cathode potential losses was due to $\eta_{[OH^-]}$.

Cathode performance in phosphate buffer

Although the above experiments were performed in unbuffered solutions, a buffer is typically used in MFCs to maintain the bulk liquid pH closer to neutral. This buffer could also help to transport OH^- from the cathode to the bulk liquid. We thus obtained polarization curves for Pt-based gas-diffusion cathodes constructed with Nafion binder in 100 mM phosphate buffer. Similar to the above experiments, we performed these experiments in buffer solutions with different pH values, ranging from 7.2 to 12.9. We show these polarization curves in Figure 3. We performed at least three replicate LSVs and show one representative set here. We provide an additional representative set in the Supporting Information as Figure S5.

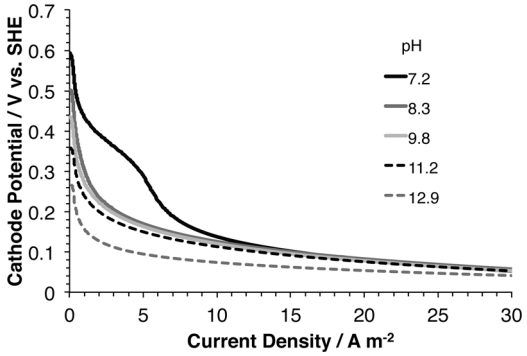

Figure 3. Polarization curves of Pt-based gas-diffusion cathodes constructed with Nafion binder in 100 mM phosphate buffer at different pH values.

Potential losses for a given current density decreased with increasing bulk liquid pH value (Figure 3). This trend is similar to the performances in unbuffered solution (Figure 1) and a result of higher $\eta_{[OH^-]}$ at lower bulk-liquid pH values. Furthermore, the phosphate buffer did not help maintaining the same local cathode pH value as the bulk liquid pH value, even at low current densities (<5 A m^{-2}), especially if the bulk pH was 8.3 or higher. This can be explained by the fact that the second pK_a value of phosphate buffer is 7.2. At a pH of 8.3 or higher, the phosphate buffer exists primarily as HPO_4^{2-} species, and, thus, a favorable gradient for transport of OH^- cannot be

obtained through the deprotonation of $H_2PO_4^-$ to HPO_4^{2-}. The local cathode pH value has to be close to the next pK_a, 12.4, for HPO_4^{2-} to deprotonate to PO_4^{3-}, to act as an OH^- carrier. However, when the cathode was in bulk liquid of pH 7.2 with buffer, the potential losses were lower in the low-current density region (<5 A m^{-2}), suggesting a benefit from the transport of OH^- through deprotonation of $H_2PO_4^-$ to HPO_4^{2-}. The use of buffer to improve cathode performance has been shown previously, although these experiments were performed at pH 3.3 and with cathodes that did not contain a gas diffusion layer;[7a] thus, it is not completely relevant to compare the relative improvement in performance with our results. In the range of 3–5 A m^{-2}, a distinct change in the slope of the polarization curve is observed, which is likely a result of the local cathode pH value reaching the third pK_a value of phosphate (i.e., 12.4). At 10 A m^{-2}, however, even the cathode in pH 7.2 solution appears to have reached a high local pH value, evident from the large potential losses at this current density.

We next compared the experimentally obtained polarization curve of the cathode in pH 7.2 solution with the η_{act}-controlled response (including η_{mixed}) of the cathode as determined by using Equation (5). We show this comparison in Figure 4. The

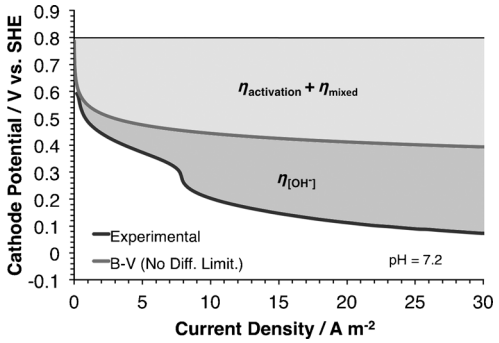

Figure 4. Comparison of a polarization curve of a Pt-based gas-diffusion cathode constructed with Nafion binder in 100 mM phosphate buffer at pH 7.2 with curves predicted from the Butler–Volmer equation without OH^- diffusion limitation.

difference between the two provides a measure of $\eta_{[OH^-]}$. At a current density of 10 A m^{-2}, $\eta_{[OH^-]}$ was >0.3 V, suggesting that the local cathode pH value was already around five units higher than the bulk liquid pH value. $\eta_{[OH^-]}$ increased only marginally beyond this current density, as expected from the results in pH 12.9 solution. $\eta_{[OH^-]}$ was smaller at low current densities (<5 A m^{-2}), but still represented a significant potential loss. For example, $\eta_{[OH^-]}$ was around 0.15 V at 4 A m^{-2}, corresponding to a local cathode pH of approximately 9.7. This pH value represents the tail end of where a favorable concentration gradient could exist for OH^- transport through deprotonation of $H_2PO_4^-$ to HPO_4^{2-}.

Cathode performance in unbuffered solution with anionomer binder

Having established that Nafion provides significant resistance to OH^- transport, either directly or through phosphate buffer as OH^- carrier, we hypothesized that replacing Nafion with an anion-conducting polymer will result in improved cathode performance through a lower $\eta_{[OH^-]}$ due to a higher D_{OH^-} as well as D_{buffer}. Several polymers containing quaternary ammonium moieties have a good anion exchange capacity and are available from applications in anion exchange membrane (AEM) fuel cells.[23] We selected one of these, AS-4 (Tokuyama Corporation), to validate our hypothesis. This particular polymer has one of the highest anion exchange capacities of all anionomers developed so far.[24]

We obtained polarization curves for Pt-based gas-diffusion cathodes constructed with AS-4 binder in unbuffered 100 mM $NaClO_4$ solution at pH 7.2, 10.8, or 13, similar to our previous experiments with cathodes constructed with Nafion binder. We show the results in Figure 5 as one representative set out of at

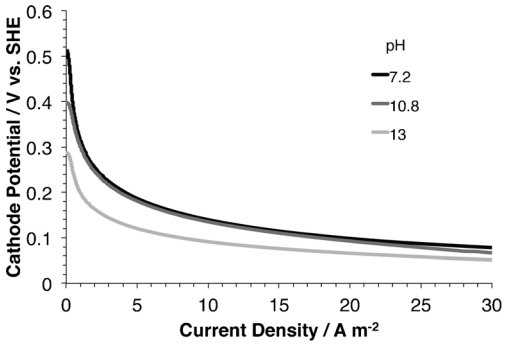

Figure 5. Polarization curves of Pt-based gas-diffusion cathodes constructed with AS-4 binder in 100 mM $NaClO_4$ solution at different pH values.

least three LSVs for each condition and we provide a replicate as Figure S6 in the Supporting Information. Similar to the cathodes with Nafion binder, the potential losses at any given current density decreased with increasing pH, suggesting that, despite the presence of a different binder, $\eta_{[OH^-]}$ developed in cathodes placed in solutions with lower pH values. However, we observed a key difference for cathodes with AS-4 binder compared to those with Nafion binder. The latter converged to the same potential at current densities of approximately 20 A m^{-2} irrespective of the bulk liquid pH value; however, in the case of AS-4 binder, the cathodes in pH 7.2 and 10.8 solutions did not converge with the cathode in pH 13 solution, even at 30 A m^{-2}. This difference indicates an improvement in OH^- transport. To confirm that the intrinsic property of the cathode catalyst had not changed, we fitted the polarization curve for the cathodes in pH 13 solution ($n=3$) to the Tafel equation and obtained values of j_0 and α of 2.8×10^{-6} A cm^{-2} and 0.143, respectively (Figure S7). Although these values are slightly different from those determined for the cathodes with Nafion binder, they still lie in the range we would expect for Pt for the ORR.[22]

Next, we used the j_0 and α values determined above to predict the η_{act}-controlled response (including η_{mixed}) of the cathode in pH 7.2 solution using Equation (5). We show this in Figure 6. Similar to the cathodes with Nafion binder, the actual response of the cathode was controlled by an additional overpotential, $\eta_{[OH^-]}$. By using Equations (5), (6), and (9), we determined the local concentration of OH^-, which showed that the local cathode pH value increased rapidly. Compared to the cathode with Nafion binder, the cathode with AS-4 binder was able to maintain only a marginally lower local cathode pH at a given current density. We further fitted the local cathode pH value of the latter to Fick's law and we observed a good fit (Figure 2) for D_{OH^-}/L of 0.00058 cm s^{-1}. This is around 60% higher than the value we determined earlier for the cathode with Nafion binder; thus, replacing Nafion with AS-4 as the binder improved OH^- transport. The magnitude of this improvement (60%) may appear large, but the relative benefit in decreasing $\eta_{[OH^-]}$ was negligible because $\eta_{[OH^-]}$ can be decreased by around 60 mV when D_{OH^-}/L is increased by a factor of 10; thus, maintaining a pH value close to neutral would require increasing D_{OH^-} for the binder approximately 10^5 times.

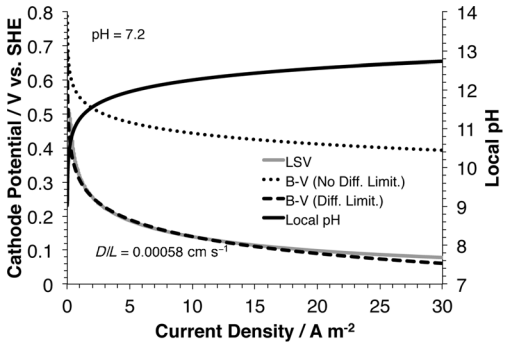

Figure 6. Comparison of a polarization curve of a Pt-based gas-diffusion cathode constructed with AS-4 binder in 100 mM $NaClO_4$ solution at pH 7.5 with curves predicted from the Butler–Volmer equation without and with OH^- diffusion limitation, and the predicted local cathode pH value as a function of current density resulting from OH^- diffusion limitation.

Cathode performance in phosphate buffer with anionomer binder

Although the anion-conducting binder we tested here did not seem to provide significant benefits over Nafion purely from the perspective of direct OH^- transport, we hypothesized that it still could allow better transport of phosphate buffer as the OH^- carrier. We thus obtained polarization curves for Pt-based gas-diffusion cathodes constructed with AS-4 binder in 100 mM phosphate buffer at pH 7.2 and compared them to those for cathodes constructed with Nafion binder. We show this comparison in Figure 7 as one representative set out of at least three LSVs for each cathode. We provide a replicate curve as Figure S8 in the Supporting Information. Compared to the cathodes with Nafion binder, potential losses for the cathode with AS-4 binder were lower. As we expect η_{act} to be the same

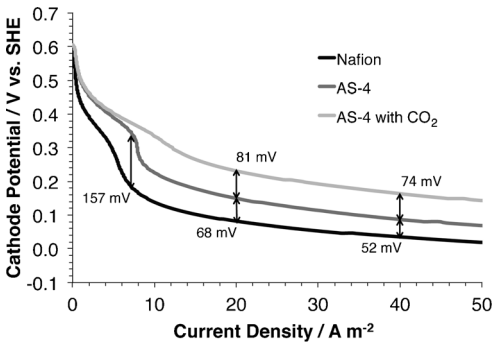

Figure 7. Comparison of polarization curves of Pt-based gas-diffusion cathode constructed with Nafion and AS-4 binders, the latter with and without CO_2 feed to the cathode, in 100 mM phosphate buffer at pH 7.2.

for both cathodes, the improved performance of the cathode with AS-4 binder is a direct result of a decrease in $\eta_{[OH^-]}$. Within the range of current densities typically observed in MFCs, $\eta_{[OH^-]}$ for the cathode with AS-4 binder was up to 157 mV lower than that for the cathode with Nafion binder, indicating a significant improvement in D/L for the phosphate buffer. Considering this result, we suggest that Nafion as the cathode catalyst binder in MFCs be replaced with anion-conducting binders such as the one we used here.

The maximum saving in $\eta_{[OH^-]}$ of 157 mV at 7.5 A m^{-2} suggests that the local cathode pH value was about 2.6 units lower with the AS-4 binder. As the cathode with the Nafion binder was close to a local pH 12 at this current density (as we determined previously), the local cathode pH value with AS-4 binder was approximately 9.4. This still represents a significant remaining $\eta_{[OH^-]}$ ($\approx$140 mV) and, thus, opportunity to improve the cathode performance remains. One of the ways that this could be achieved is by using anion-conducting binders with higher anion exchange capacities, such as those containing quaternary phosphonium groups. These have shown anion exchange capacities at least 2–3 times those of polymers containing quaternary ammonium groups.[25]

A second way to improve cathode performance would be through providing additional buffer in the form of CO_2. We have shown in the past that adding CO_2 to the cathode chamber in MFCs containing a membrane helps to transport OH^- across the membrane.[26] Similarly, adding CO_2 even in membrane-less systems should allow enhanced OH^- transport from the cathode catalyst to the bulk liquid. H_2CO_3 (hydrated CO_2) would deprotonate to HCO_3^-, thus acting as an OH^- carrier. The advantage of providing CO_2, especially to gas-diffusion cathodes, is that it can be delivered directly to the catalyst sites through the gas-diffusion layer, compared to phosphate buffer, which suffers from the same diffusion limitations as OH^-. Also, the second pK_a of the CO_2 buffer system is 10.3, which would allow a lower cathode pH value to be maintained at higher current densities than phosphate through OH^- transport by the HCO_3^-/CO_3^{2-} couple. We thus obtained polarization curves for the cathodes constructed with AS-4 binder with CO_2 feed (5% mixture with air). We show a representative curve in Figure 7. It is apparent that CO_2 addition did not sig-

nificantly help in the region of low current densities ($<5\ A\,m^{-2}$) as phosphate was already partially aiding OH^- transport, and thus $\eta_{[OH^-]}$ was small. However, CO_2 addition resulted in lower $\eta_{[OH^-]}$ at higher current densities. Compared to the cathode with Nafion (and no CO_2), $\eta_{[OH^-]}$ was around 120–140 mV lower for the cathode with AS-4 with CO_2 addition, thus representing a local cathode pH value close to 10. We thus conclude that enhanced OH^- transport occurred through the deprotonation of H_2CO_3 to CO_3^{2-}.

Our cumulative results clearly indicate the importance of OH^- transport from cathodes in MFCs. Although we report values of potential losses here specifically for gas-diffusion cathodes as they are used in single-chamber MFCs, our findings related to OH^- transport limitations also should apply to all MFCs with a cathode containing a polymer binder and/or surrounded by bulk electrolyte at neutral pH as well as to enzymatic fuel cells that use an abiotic cathode under similar conditions. We have shown that replacing Nafion as the catalyst binder with an anion-conducting binder and providing CO_2 to the cathode as an additional OH^- carrier improves OH^- transport, thus reducing $\eta_{[OH^-]}$. Although we used gas-diffusion half cells and thus cannot demonstrate directly the effect of improving OH^- transport on power densities in MFCs, we can estimate these by using a realistic case. We assume an MFC with equally sized electrodes, with an anode producing $7.5\ A\,m^{-2}$ at -0.1 V versus SHE. At this current density, the cathode potentials would be 0.176 V versus SHE with Nafion binder and 0.333 V versus SHE with AS-4 binder. We need to estimate the Ohmic losses for this system, which we do by assuming using a 100 mM phosphate buffer (conductivity of $\approx 15\ mS\,cm^{-1}$) and a distance of 2 cm between the anode and the cathode, as is typically used in laboratory MFCs; this gives an Ohmic loss of around 0.1 V. Hence, the MFC with the cathode with Nafion binder would produce a power density of $1.3\ W\,m^{-2}$, which is similar to those obtained experimentally by other groups.[7d,17a,c,27] In comparison, the cathode with AS-4 binder would produce a power density of $2.5\ W\,m^{-2}$. This constitutes an increase in power density of $>90\%$ strictly achieved by replacement of the cathode catalyst binder.

Conclusions

We have shown here that sluggish transport of OH^- from the cathode catalyst layer to the bulk liquid results in considerable potential losses in microbial fuel cell (MFC) cathodes. For gas-diffusion cathodes, we determined the combined D_{OH^-}/L value for the cathode catalyst layer and the diffusion boundary layer at the interface with the bulk liquid to be $0.00034\ cm\,s^{-1}$, confirming that the use of Nafion as the catalyst binder significantly impedes OH^- transport. We also determined that phosphate buffer does not help maintaining a neutral cathode pH value. At a current density of $10\ A\,m^{-2}$, this pH-based potential loss was >0.3 V, representing a significant fraction of the overall cathodic potential loss.

We also showed that replacing the Nafion binder with an anion-conducting binder, here AS-4, partially improved cathode performance through an increase in D_{OH^-}/L to $0.00058\ cm\,s^{-1}$ as well as improved transport of buffer species. At a current density of $7.5\ A\,m^{-2}$, potential losses with AS-4 binder were approximately 157 mV lower than those with Nafion binder, representing a decrease in local cathode pH value by around 2.6 units. The pH-based potential loss can be decreased further, especially for high current densities, by providing CO_2 directly to the cathode as an acid. This occurs as a result of buffering close to pH 10.3 (second pK_a of the carbonate species), compared with the phosphate buffer only, for which the relevant pK_a is 12.4.

Experimental Section

Cathodes

We prepared cathodes ($9\ cm^2$) from 30% wet-proofed carbon cloth gas-diffusion layers coated with a microporous carbon layer (MPCL) on one side (Electrochem Inc., USA). We prepared catalyst ink using 0.5 g of 30% Pt/C powder (Electrochem Inc., USA) mixed in 5 mL of 5% ionomer in isopropanol solution (Nafion, Sigma–Aldrich, USA, or AS-4, Tokuyama Corporation, Japan) by sonication for 30 min and magnetic stirring for 24 h, as binder, and applied it to the side of cathodes opposite to the MPCL by using a paint brush. We used a Pt loading of $0.5\ mg\,cm^{-2}$ on all cathodes.

Gas-diffusion half cells

We constructed gas-diffusion half cells (3 cm × 1.8 cm × 3 cm) as Plexiglass chambers of around 16 mL volume closed at one end. We placed the cathodes at the other end with the catalyst-coated side facing inside (towards the solution) and the MPCL outside (towards air). We used a saturated calomel electrode (+0.244 V vs. SHE) as the reference electrode and placed it inside the cells at a distance of 5 mm from the cathode. We used a stainless steel rod as the counter electrode ($\approx 9\ cm^2$, 5 mm diameter). We obtained LSVs for the cathodes in 100 mM phosphate buffer, prepared with 65 mM Na_2HPO_4 and 35 mM $NaH_2PO_4{\cdot}H_2O$, and adjusted the buffer solution to pH values of 7.2, 8.3, 9.8, 11.2, and 12.9 by using different amounts of 4 M NaOH. We also conducted experiments in the absence of buffer using 100 mM $NaClO_4$ in deionized water, adjusting the pH values to 7.2 (or 7.5), 10.8, and 13 by using different amounts of 4 M NaOH. We also conducted some experiments with CO_2 fed to the cathode mixed with air at concentrations of 5%. For these experiments, we added a Plexiglass chamber to the cathode side to which we fed the gas mixture at a flow rate of $100\ mL\,min^{-1}$.

Electrochemical analyses

We performed LSVs on all cathodes at 30 °C by using a potentiostat (Princeton Applied Research, USA) at a scan rate of $1\ mV\,s^{-1}$. We performed *iR* correction for all LSVs to correct for the Ohmic loss between the reference electrode and the cathode, by using an average Ohmic loss as measured from around 20 impedance spectroscopy measurements at 100 kHz with an amplitude of 10 mV. For each condition and/or cathode, we obtained at least three polarization curves. We also obtained *j–V* curves for selected cathodes and conditions using chronopotentiometry to confirm that a steady state was achieved in the LSVs at the selected scan rate.

Acknowledgements

We thank the United States Office of Naval Research for funding (N00014-10M-0231) and Tokuyama Corporation, Japan, for providing the AS-4 anionomer. We also thank Dr. Andrew Kato Marcus for useful discussions and comments.

Keywords: bacteria · cathodes · electrochemistry · fuel cells · oxygen reduction

[1] a) K. Rabaey, W. Verstraete, *Trends Biotechnol.* **2005**, *23*, 291 – 298; b) B. E. Logan, B. Hamelers, R. A. Rozendal, U. Schröder, J. Keller, S. Freguia, P. Aelterman, W. Verstraete, K. Rabaey, *Environ. Sci. Technol.* **2006**, *40*, 5181 – 5192; c) B. E. Logan, *Appl. Microbiol. Biotechnol.* **2010**, *85*, 1665 – 1671; d) P. Clauwaert, D. van der Ha, N. Boon, K. Verbeken, M. Verhaege, K. Rabaey, W. Verstraete, *Environ. Sci. Technol.* **2007**, *41*, 7564 – 7569; e) S. R. Higgins, C. Lau, P. Atanassov, S. D. Minteer, M. J. Cooney, *ACS Catal.* **2011**, *1*, 994 – 997.

[2] a) L. T. Angenent, K. Karim, M. H. Al-Dahhan, R. Domiguez-Espinosa, *Trends Biotechnol.* **2004**, *22*, 477 – 485; b) Z. W. Du, H. R. Li, T. Y. Gu, *Biotechnol. Adv.* **2007**, *25*, 464 – 482; c) R. A. Rozendal, H. V. M. Hamelers, K. Rabaey, J. Keller, C. J. N. Busiman, *Trends Biotechnol.* **2008**, *26*, 450 – 459; d) J. J. Fornero, M. Rosenbaum, L. T. Angenent, *Electroanalysis* **2010**, *22*, 832 – 843.

[3] a) C. I. Torres, A. K. Marcus, B. E. Rittmann, *Biotechnol. Bioeng.* **2008**, *100*, 872 – 881; b) A. E. Franks, K P. Nevin, H. F. Jia, M. Izallalen, T. L. Woodard, D. R. Lovley, *Energy Environ. Sci.* **2009**, *2*, 113 – 119.

[4] a) B. H. Kim, I. S. Chang, G. M. Gadd, *Appl. Microbiol. Biotechnol.* **2007**, *76*, 485 – 494; b) P. Clauwaert, P. Aelterman, T. H. Pham, L. De Schamphelaire, M. Carballa, K. Rabaey, W. Verstraete, *Appl. Microbiol. Biotechnol.* **2008**, *79*, 901 – 913.

[5] a) C. I. Torres, A. K. Marcus, P. Parameswaran, B. E. Rittmann, *Environ. Sci. Technol.* **2008**, *42*, 6593 – 6597; b) E. Marsili, J. B. Rollefson, D. B. Baron, R. M. Hozalski, D. R. Bond, *Appl. Environ. Microbiol.* **2008**, *74*, 7329 – 7337; c) C. I. Torres, A. K. Marcus, H. S. Lee, P. Parameswaran, R. Krajmalnik-Brown, B. E. Rittmann, *FEMS Microbiol. Rev.* **2010**, *34*, 3 – 17.

[6] S. Chen, H. Hou, F. Harnisch, S. A. Patil, A. A. Carmona-Martinez, S. Agarwal, Y. Zhang, S. Sinha-Ray, A. L. Yarin, A. Greiner, U. Schröder, *Energy Environ. Sci.* **2011**, *4*, 1417 – 1421.

[7] a) F. Zhao, F. Harnisch, U. Schröder, F. Scholz, P. Bogdanoff, I. Hermann, *Environ. Sci. Technol.* **2006**, *40*, 5193 – 5199; b) H. Rismani-Yazdi, S. M. Carver, A. D. Christy, I. H. Tuovinen, *J. Power Sources* **2008**, *180*, 683 – 694; c) Y. Z. Fan, E. Sharbrough, H. Liu, *Environ. Sci. Technol.* **2008**, *42*, 8101 – 8107; d) S. Cheng, B. E. Logan, *Bioresour. Technol.* **2011**, *102*, 4468 – 4473.

[8] R. A. Robinson, R. H. Stokes, *Electrolyte Solutions*, Butterworths, London, **1959**.

[9] C. H. Hamann, A. Hamnett, W. Vielstich, *Electrochemistry*, Wiley-VCH, Weinheim, **1998**.

[10] J. R. Varcoe, R. C. T. Slade, *Fuel Cells* **2005**, *5*, 187 – 200.

[11] a) V. Jovancicevic, J. O'M. Bockris, *J. Electrochem. Soc.* **1986**, *133*, 1797 – 1807; b) F. King, C. D. Litke, Y. Tang, *J. Electroanal. Chem.* **1995**, *384*, 105 – 113; c) A. Prieto, J. Hernandez, E. Herrero, J. M. Feliu, *J. Solid State Electrochem.* **2003**, *7*, 599 – 606.

[12] D. Natarajan, T. V. Nguyen, *J. Power Sources* **2003**, *115*, 66 – 80.

[13] F. Harnisch, U. Schröder, *ChemSusChem* **2009**, *2*, 921 – 926.

[14] R. A. Rozendal, H. V. M. Hamelers, C. J. N. Buisman, *Environ. Sci. Technol.* **2006**, *40*, 5206 – 5211.

[15] S. Cheng, H. Liu, B. E. Logan, *Environ. Sci. Technol.* **2006**, *40*, 364 – 369.

[16] P. Piela, P. K. Wrona, *J. Power Sources* **2006**, *158*, 1262 – 1269.

[17] a) T. Saito, M. D. Merrill, V. J. Watson, B. E. Logan, M. A. Hickner, *Electrochim. Acta* **2010**, *55*, 3398 – 3403; b) Y. L. Huang, Z. He, F. Mansfeld, *Bioelectrochemistry* **2010**, *79*, 261 – 264; c) T. Saito, T. H. Roberts, T. E. Long, B. E. Logan, M. A. Hickner, *Energy Environ. Sci.* **2011**, *4*, 928 – 934.

[18] *CRC Handbook of Chemistry and Physics*, 87th edition (Ed.: D. R. Lide), CRC Press, Cleveland, **2006**.

[19] R. O'Hayre, S. W. Cha, W. Colella, F. B. Prinz, *Fuel Cell Fundamentals*, Wiley, New York, **2006**.

[20] a) Z. H. Wang, C. Y. Wang, K. S. Chen, *J. Power Sources* **2001**, *94*, 40 – 50; b) M. Ciureanu, R. Roberge, *J. Phys. Chem. B* **2001**, *105*, 3531 – 3539; c) S. Um, C. Y. Wang, *J. Power Sources* **2004**, *125*, 40 – 51.

[21] F. Harnisch, S. Wirth, U. Schröder, *Electrochem. Commun.* **2009**, *11*, 2253 – 2256.

[22] a) A. Damjanovic, V. Brusic, *Electrochim. Acta* **1967**, *12*, 615 – 628; b) D. B. Sepa, V. Vojnovic, A. Damjanovic, *Electrochim. Acta* **1981**, *26*, 781 – 793; c) A. Parthasarathy, C. R. Martin, S. Srinivasan, *J. Electrochem. Soc.* **1991**, *138*, 916 – 921; d) A. Parthasathy, S. Srinivasan, A. J. Appleby, C. R. Martin, *J. Electrochem. Soc.* **1992**, *139*, 2530 – 2537.

[23] a) J. R. Varcoe, R. C. T. Slade, *Electrochem. Commun.* **2006**, *8*, 839 – 843; b) J. Fang, P. K. Shen, *J. Membr. Sci.* **2006**, *285*, 317 – 322; c) Y. Xiong, J. Fang, Q. H. Zeng, Q. L. Liu, *J. Membr. Sci.* **2008**, *311*, 319 – 325.

[24] H. Yanagi, K. Fukuta, *ECS Trans.* **2008**, *16*, 257 – 262.

[25] a) S. Gu, R. Cai, T. Luo, Z. Chen, M. Sun, Y. Liu, G. He, Y. Yan, *Angew. Chem.* **2009**, *121*, 6621 – 6624; *Angew. Chem. Int. Ed.* **2009**, *48*, 6499 – 6501; b) S. Gu, R. Cai, T. Luo, K. Jensen, C. Contreras, Y. S. Yan, *ChemSusChem* **2010**, *3*, 555 – 558.

[26] C. I. Torres, H. S. Lee, B. E. Rittmann, *Environ. Sci. Technol.* **2008**, *42*, 8773 – 8777.

[27] a) X. Wang, S. A. Cheng, Y. J. Feng, M. D. Merrill, T. Saito, B. E. Logan, *Environ. Sci. Technol.* **2009**, *43*, 6870 – 6874; b) Y. J. Feng, Q. Yang, X. Wang, B. E. Logan, *J. Power Sources* **2010**, *195*, 1841 – 1844; c) F. Zhang, T. Saito, S. A. Cheng, M. A. Hickner, B. E. Logan, *Environ. Sci. Technol.* **2010**, *44*, 1490 – 1495.

Received: November 30, 2011
Revised: February 5, 2012
Published online on May 21, 2012

DOI: 10.1002/cssc.201100748

On Electron Transport through *Geobacter* Biofilms

Daniel R. Bond,[b] Sarah M. Strycharz-Glaven,[a] Leonard M. Tender,*[a] and César I. Torres[c, d]

Geobacter spp. can form a biofilm that is more than 20 μm thick on an anode surface by utilizing the anode as a terminal respiratory electron acceptor. Just how microbes transport electrons through a thick biofilm and across the biofilm/anode interface, and what determines the upper limit to biofilm thickness and catalytic activity (i.e., current, the rate at which electrons are transferred to the anode), are fundamental questions attracting substantial attention. A significant body of experimental evidence suggests that electrons are transferred from individual cells through a network of cytochromes associated with cell outer membranes, within extracellular polymeric substances, and along pili. Here, we describe what is known about this extracellular electron transfer process, referred to as electron superexchange, and its proposed role in biofilm anode respiration. Superexchange is able to account for many different types of experimental results, as well as for the upper limit to biofilm thickness and catalytic activity that *Geobacter* biofilm anodes can achieve.

Introduction

*Geobacter spp. (*e.g., *Geobacter sulfurreducens* strain DL1) can acquire energy by coupling the intracellular oxidation of organic matter, such as acetate, with extracellular electron transfer to an anode (an electrode maintained at a sufficiently positive electrochemical potential to act as an electron drain) resulting in an electric current (Figure 1).[1] The anode-respiring ability of *Geobacter* derives from their ability to reduce insoluble oxidants, such as Fe^{III} oxides, observed in natural environments.

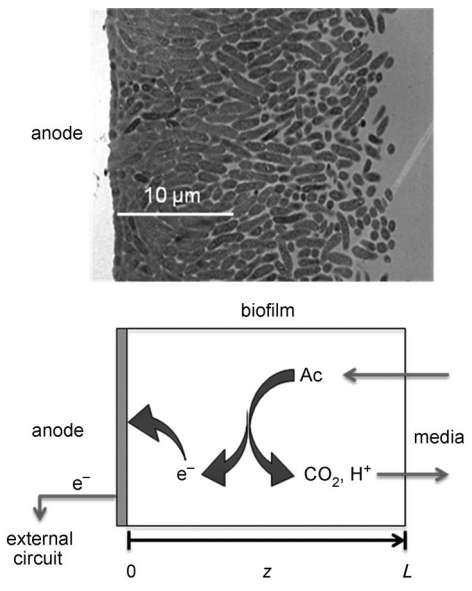

Figure 1. Top: TEM image of cross section of *Geobacter sulfurreducens* strain DL-1 biofilm anode grown to the point where growth becomes limited (image courtesy of E. V. LaBelle). Bottom: Schematic depiction of the overall process of *Geobacter* biofilm anode respiration. Here, acetate is the electron donor, *L* is the biofilm thickness (typically > 20 μm), and *z* is the distance from the anode surface inside the biofilm.

Although other species are known to catalyze anodic reactions,[2] *Geobacter* are distinct for the high rate at which they can directly transfer electrons to an anode surface, comparable to the rate at which they can respire soluble oxidants such as Fe^{III} citrate, while not relying on soluble electron transfer mediators such as flavins.[3] Furthermore, on anodes that are inexhaustible electron acceptors, *Geobacter* can form multi-microbe thick, persistent biofilms not observed when respiring insoluble oxidants, in which microbes residing more than 20-cell lengths away utilize the anode as their terminal electron acceptor. The combination of robust direct electron transfer and high cell surface density (microbes across the entire biofilm generating electrons, which are collected by the underlying anode) enables *Geobacter* biofilms to achieve higher anodic current densities than any other species.[4] For this reason, *Geobacter* may play an important role in emerging technologies based on microbe-catalyzed anode processes for which abiotic catalysts do not exist, such as wastewater treatment and energy generation from biomass oxidation.[5]

[a] *Dr. S. M. Strycharz-Glaven, Dr. L. M. Tender*
Naval Research Laboratory
Center for Bio/Molecular Science and Engineering
Washington, DC 20375 (USA)
E-mail: tender@nrl.navy.mil

[b] *Prof. D. R. Bond*
BioTechnology Institute and Department of Microbiology
University of Minnesota
St. Paul, MN 55108 (USA)

[c] *Prof. C. I. Torres*
Swette Center for Environmental Biotechnology
The Biodesign Institute at Arizona State University
P.O. Box 875701, Tempe, AZ 85287-5701 (USA)

[d] *Prof. C. I. Torres*
School for Engineering of Matter, Transport and Energy
Arizona State University
501 E Tyler Mall, Tempe, AZ 85287 (USA)

Evidence that superexchange controls biofilm anode electron transport

How cells and cellular components coordinate in the transport of electrons through a thick biofilm and across the biofilm/anode interface and what limits the rate and distance that electrons can be transported through an anode respiring biofilm are unresolved. Cyclic voltammetry,[3,6] conductivity measurements,[7] and spectroelectrochemical measurements[8] performed on living, actively respiring biofilms all indicate that *Geobacter* biofilm anodes contain discrete, biofilm-bound redox cofactors that are reversibly oxidized and reduced in response to the anode potential. The key observation from all three types of experiments is that the transport of electrons through a *Geobacter* biofilm anode exhibits diffusive behavior characterized by Fick's laws of diffusion,[6a,d,7,9] consistent with extracellular electron transport involving sequential electron-transfer self-exchange reactions (i.e., electron hopping) between discrete redox cofactors in a manner resembling an electron "bucket brigade".

We refer to this form of extracellular electron transport in *Geobacter* biofilm anodes as electron superexchange, in deference to the established use of this term to describe this form of electron transport within redox hydrogels including wired enzyme electrodes.[10] Based on superexchange, the driving force for extracellular electron transport toward the anode surface during anode respiration is the effective concentration gradient of electrons across the biofilm (i.e., a redox gradient), arising from the reduction of oxidized cofactors by microbes within the biofilm, and oxidation of reduced cofactors at the anode surface.[6d,7,9b] Accordingly, the local rate of electron transport at any given location inside the biofilm, including at the biofilm/anode interface, resulting in current is expected to be proportional to the local concentration gradient of reduced cofactor (Fick's 1st law of diffusion).

In the case of cyclic voltammetry, a set of transient anodic and cathodic voltammetric current peaks are observed for living, actively respiring *Geobacter* biofilms grown on anodes at sufficiently fast scan rates (typically $>0.02\ V\,s^{-1}$).[6c,9b] These peaks result from the change in oxidation state of redox cofactors within the biofilm in response to the changing anode potential, and the potentials at which these peaks occur [at approximately -0.2 V vs. standard hydrogen electrode (SHE)] are similar to the formal potentials of known *c*-type cytochromes purified from *G. sulfurreducens*.[11] In electrochemistry, the term pseudocapacitance is used to describe the charge (the integral of current over time) associated with such voltammetric peaks; a more thorough description of which is available.[6d] In all published studies, these voltammetric peaks scale in magnitude with the square root of the voltammetric scan rate. This observation indicates that a diffusive process (referred to as semi-infinite diffusion in a confined film[6d]) consistent with superexchange, governs the transport of electrons between biofilm redox cofactors and the anode surface as the oxidation state of the cofactors changes in response to the changing anode potential. Moreover, the formal potentials of these voltammetric peaks are centered on the midpoint potential of the sigmoid-shaped catalytic current–electrode potential dependency (i.e., catalytic voltammetry) observed at slower scan rates (typically $<0.02\ V\,s^{-1}$). This is consistent with a catalytic current limited by the rate at which cells deliver electrons to redox cofactors in the biofilm that subsequently transport electrons to the anode surface via superexchange, as determined by modeling *Geobacter* biofilm anodes as enzyme-functionalized electrodes (in the absence of pH considerations, vide infra).[9b] Voltammetric peaks observed in the absence of acetate (non-turnover condition) are also centered at the same approximate formal potential as when acetate is present, indicating that the same electron transport process observed by voltammetry of resting cells is involved in anode respiration.[9b]

In the case of spectroelectrochemistry,[8b,c] diffusive electron-transport behavior consistent with superexchange is also exhibited by actively respiring *Geobacter* biofilm anodes. Here, a lag in the change of oxidation state of biofilm redox cofactors, specifically *c*-type cytochromes (vide infra), is observed spectroscopically while the electrode potential is changed during voltammetry. This lag increases in duration with increasing voltammetric scan rate and increasing biofilm thickness. As above, this observation indicates that a diffusive electron transport process governs the transport of electrons between biofilm redox cofactors and the anode surface, where the time required for electrons to radiate via superexchange across the biofilm becomes more apparent the faster the electrode potential is changed and the thicker the biofilm becomes.

In the case of conductivity measurements,[7] diffusive electron transport behavior consistent with superexchange is also exhibited by actively respiring *Geobacter* biofilm anodes. Here, a sigmoid-shaped dependency (rather than a linear dependency) is observed for a current conducted through a *Geobacter* biofilm connecting two separated electrodes as voltage is applied to the electrodes.[7]

These independent measurements (electrochemical, spectral, and conductance) performed on actively respiring *Geobacter* biofilm anodes all yield results highly characteristic of systems for which long-range electron transport results from electron transfer reactions between discrete redox cofactors. This results in diffusive-like electron transport behavior consistent with known systems for which electron transport occurs via superexchange.[10]

Evidence for the role of *c*-type cytochromes

G. sulfurreducens cells possess an abundance of multiheme *c*-type cytochromes on their outer membrane, in extracellular polymeric substances, and along pili.[11a,b,12] *C*-type cytochromes are ubiquitous redox proteins involved in biological electron-transport processes, but are best known for systems in which single or diheme cytochromes shuttle electrons between larger electron transfer proteins.[13] In contrast, multiheme *c*-type cytochromes can act as immobilized electron conduits spanning large distances, as has been demonstrated for the *Shewanella* CymA-MtrA-MtrC system,[14] where three multiheme cytochromes transfer electrons from the inner membrane to the outer surface in a sequence of 24 interacting hemes.

Spectroelectrochemistry specifically implicates cytochromes as the dominant redox cofactors involved in *Geobacter* biofilm extracellular electron transfer. Four different laboratories have used UV-Vis absorption spectroscopy,[8] surface-enhanced infrared absorption spectroscopy,[15] and surface-enhanced Raman spectroscopy[16] combined with electrochemistry to investigate *Geobacter* biofilm anodes, demonstrating characteristic spectra of *c*-type cytochromes that undergo changes in oxidation state with changes in the anode potential. Furthermore, Liu and Bond[8c] found a linear increase in catalytic current with the amount of *c*-type cytochrome in a *Geobacter* biofilm anode during biofilm growth, consistent with electrochemical data,[6d] demonstrating a linear increase in the amount of redox cofactor in a *Geobacter* biofilm anode with catalytic current during biofilm growth. Although they may be hidden by the large signal produced by *c*-type cytochromes, no significant spectroscopic signals indicative of other potential redox cofactors with formal potentials in this range (−0.2 to −0.5 vs. SHE), such as quinones and flavins, have been detected.

Analysis of surface-enhanced Raman spectra directly implicates *c*-type cytochromes in electron-transfer across the biofilm/anode interface.[16] This evidence is further supported by the observation of multiple sets of voltammetric peaks in cyclic voltammograms recorded under non-turnover conditions (where cells have no acetate to oxidize, e.g., Figure 9B, Strycharz et al.[9b]) comparable to that observed for isolated multiheme *c*-type cytochromes involved in electron transport of *Shewanella oneidensis* strain MR-1.[14b,c] Such peaks are consistent with the presence of a multi-electron accepting redox cofactor at the biofilm/anode interface, whose formal potential is influenced by the number of transient electrons residing in the cofactor due to repulsive electron–electron interactions (i.e., a Coulomb blockade).[9a] Prior modeling indicates that the formal potential of redox cofactors involved in electron transfer across the biofilm/anode interface cannot be more negative than the midpoint potential of the catalytic voltammetry (e.g., Figure 9A in Ref. [9b]), suggesting that during anode respiration, only one transient electron at a time may reside in multiheme *c*-type cytochromes transferring electrons to the anode.

Genetic data is less definitive with respect to implicating cytochromes as redox cofactors involved in biofilm anode electron transfer, as deletion of certain *G. sulfurreducens* cytochromes leads to multiple changes in expression of other cytochromes and proteins.[17] Perhaps the most compelling evidence involves the octoheme cytochrome OmcZ. This protein is secreted outside the cell, where it is loosely tethered to material extending far beyond the outer membrane.[12f,18] Consistent with its possible role as an extracellular electron transfer agent, OmcZ tends to aggregate to itself, is highly stable, and has a reduction potential of approximately −0.22 V versus SHE, consistent with thermodynamics of anode respiration (vide infra). Further, deletion of OmcZ eliminates the ability of *G. sulfurreducens* to utilize anodes as electron acceptors. Many other cytochromes, such as those shown to be organized along pili (OmcS), loosely attached to the outer surface (OmcE), or attached to the outer membrane (OmcB), also produce phenotypes in anode-grown biofilms,[6c] but these mutants tend to select for suppressor mutants able to express other cytochromes, which complicates the study of their specific roles.[17,19]

Scheme of biofilm-anode catalytic activity

A schematic depiction of the proposed catalytic process, including the superexchange extracellular electron-transport process that incorporates the results described above, is shown in Scheme 1. Details of independent components of this Scheme

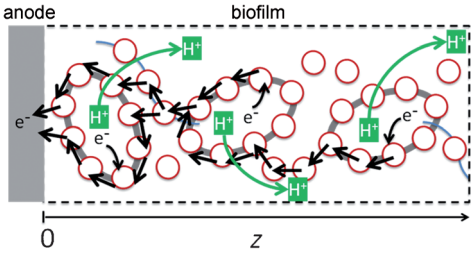

Scheme 1. Schematic depiction of *Geobacter* biofilm anode respiration at the microbe layer. Here, biofilm-bound redox cofactors (*c*-type cytochromes) associated with cell surfaces, along pili, and within extracellular polymeric substances act as extracellular terminal electron acceptors for cells metabolizing acetate, as well as mediators facilitating electron-transport through the biofilm by self-exchange among adjacent cofactors, and ultimately as the electron donors for electron transfer to the anode surface resulting in electrical current. Concomitantly generated protons diffuse out of the biofilm, in the opposite direction of electron flow, toward adjacent media.

have been described extensively elsewhere.[4,7,9b,20] Here, for a given microbe in the biofilm, electrons resulting from intracellular acetate oxidation are transported from the cytoplasm to outer membrane cytochromes associated with the microbe. Once in the extracellular environment, electrons are transferred between cytochromes, either on cell outer membranes, aligned along pili,[12c] or in the extracellular polymeric substances,[12f] until they reach cytochromes associated with microbes at the biofilm/anode interface, where they are transferred to the anode (referred to as a heterogeneous electron transfer reaction as it involves an electrode). Concomitantly generated protons diffuse complexed with bases toward the media.

The following are key aspects of this scheme.

Electron transport must be very efficient

Cyclic voltammetry of *Geobacter* biofilms grown utilizing acetate as the electron donor has repeatedly demonstrated a thermodynamic threshold below which *Geobacter* is unable to donate electrons to an anode; this value is approximately −0.22 V versus SHE.[3,6a,c,9b,21] Taking into account the reduction potential of the CO_2/acetate half-reaction (−0.29 V vs. SHE), this indicates that less than 0.07 V (6.7 kJ per electron) is used during cellular respiration to generate proton motive force. Thus, for the complete eight-electron oxidation of acetate under standard conditions, only 53.6 kJ per mol acetate is potentially available for all adenosine triphosphate (ATP) generation needs, a value that will be even lower as acetate concentrations are reduced. These electrochemical observations are consistent with chemostat and modeling studies concluding

that *Geobacter* obtains much less than one ATP per acetate oxidized when metals are the electron acceptor.[22] The low energy gain from anode respiration may reflect the fact that iron(III) oxyhydroxides in the environment also typically have low redox potentials, and that, when acetate and Fe^{III} are at low concentrations, conserving any additional energy would be uncompetitive.

The second important observation derived from voltammetry is that *Geobacter* only requires anodes to be poised at potentials 0.1 V higher than this thermodynamic threshold to reach its maximum rates of anode respiration. In other words, when anodes are poised at −0.10 V versus SHE, cells respire just as fast as when the anode is raised to potentials 0.5 V higher.[3a,6c,7] This observation reveals two facts: *Geobacter* does not take advantage of excess available potential energy when anodes are poised at higher potentials, and only about 0.1 V is lost while driving electron transport across multiple insulating membranes, through multiple microns of extracellular space, and across the biofilm/anode interface. Such a low energy loss is only possible if the intrinsic rate of electron self-exchange between proteins, and with the anode surface, is very fast (i.e., activation energy barriers are very low).

A calculation investigating this low energy exchange hypothesis has been performed to model electron transport between two microelectrodes spanning an extracellular fiber isolated from *Shewanella oneidensis* strain MR-1.[23] Electron transport for this organism has also been observed with very low (≈0.1–0.2 V) driving forces, which was modeled by electron superexchange among redox cofactors proposed to be associated with the fiber.[24] Electron transfer along such fibers at observed rates[23] was possible via a superexchange mechanism as long as the redox cofactors were closely spaced and the calculated activation energy for electron transfer among adjacent cofactors was among the lowest exhibited for biological electron transfer reactions (on the order of 0.6 mV).[25]

pH gradient

Proton transport is crucial within a *Geobacter* biofilm due to high stoichiometric production of protons during anode respiration:

$$CH_3COO^- + 3\,H_2O \rightarrow CO_2 + HCO_3^- + 8\,H^+ + 8\,e^- \quad (1)$$

In fact, no other microbial metabolic pathway, respiratory or fermentative, produces as many protons per substrate consumed as anode respiration because in the case of anode respiration, negative charge (electrons) is removed at the base of the biofilm. As electrons are produced and transported to the anode, concomitantly produced protons must be transported out of the biofilm and into adjacent media.[20a] Proton transport is thought to occur by diffusion[26] of protons complexed with buffers (such as carbonate and phosphate ions)[20a,26b] owing to low proton concentration at near-neutral pH values favored by *Geobacter*.

The generation of protons by cells within a *Geobacter* biofilm anode, and their diffusion out of the biofilm, is predicted to result in the formation of a proton concentration gradient across the biofilm (Figure 2). In this gradient, a drop in the pH value is expected to occur close to the biofilm/anode interface. This drop becomes more pronounced as the biofilm grows thicker. Imaging by using pH-sensitive dyes confirms that a pH gradient does occur, in which a pH value as low as 6.1 can occur close to the biofilm/anode interface of a full grown *Geo-*

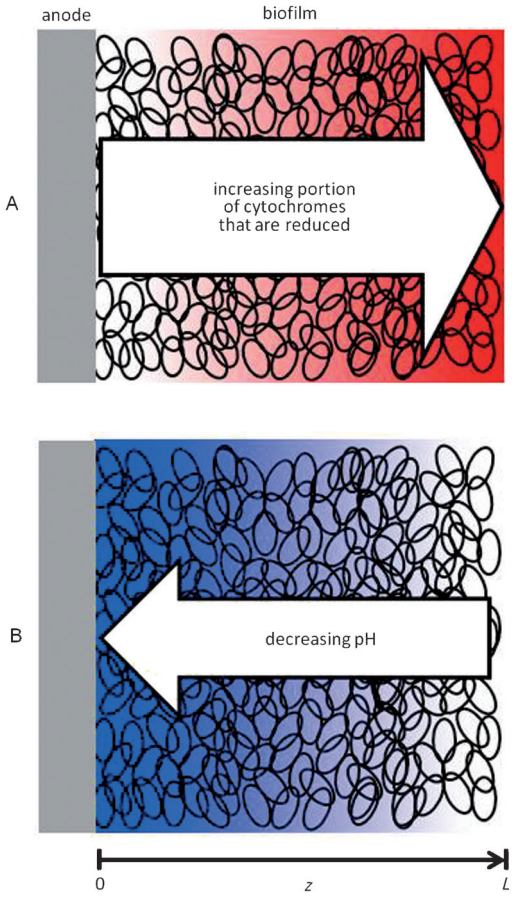

Figure 2. A) The proposed use for cytochromes in the biofilm to both accept electrons from cells they are associated with, as well as electrons transported from cells residing further from the anode surface, is predicted to result in generation of a redox gradient across the biofilm, represented by the arrow pointing away from the electrode surface. With increasing distance from the anode surface, the relative abundance of cytochromes in the oxidized state decreases while the relative abundance of cytochromes in the reduced state increases, represented here by a shift in biofilm color from white to red with increasing distance from the anode surface (*z*). In the absence of any other limitations, the biofilm will grow in thickness until the relative abundance of cytochromes in the oxidized state at the outer edge (*L*) is too low to act as electron acceptors for cells, and thus cannot support any additional biofilm growth. B) In addition, the generation of protons inside the biofilm due to anode respiration, and their transport out of the biofilm by diffusion, is expected to result in generation of the depicted pH gradient across the biofilm indicated by the arrow pointing toward the electrode surface. As the biofilm grows thicker, the pH drops further in the biofilm represented here by a shift in biofilm color from white to purple with decreasing distance from the anode surface (*z*). In the absence of any other nutritional limitations, the biofilm will grow in thickness until the rate of electron transport through the biofilm region closest to the anode surface is inhibited either by direct effects of low pH values on cytochromes, on the metabolism of cells in this low pH region, and/or on the availability of oxidized cytochromes distant from the electrode.

bacter biofilm anode,[27] a pH value known to decrease metabolic activity.[21] Such a pH gradient is expected to disproportionally affect metabolic activity of microbes closest to the biofilm/anode interface and is, therefore, expected to diminish the net contribution to current by additional cells as the biofilm grows thicker. The effect of a low pH value may be even more pronounced, creating a negative feedback loop that limits biofilm thickness, if the rate of electron transfer between adjacent cyctochromes and/or across the biofilm/anode interface itself is negatively affected by low pH values. Although little is known about the pH optima of cytochromes involved in these reactions, the distorted sigmoid-shaped current–voltage dependencies of *G. sulfurreducens* biofilm anodes recorded under conditions that exacerbate the effects of pH (e.g., Figure 6 in Torres et al.[20a]) are consistent with the hypothesis that as the pH value decreases, the rate of electron transfer across the biofilm/anode interface decreases (e.g., Figure 8 in Ref. [9b]). Decreasing the pH value has also been shown to shift the midpoint potential of cytochromes within the extracellular matrix positively by approximately 50 mV for each pH unit (close to the theoretical Nernstian value of 0.059 V per pH unit), which would reduce the driving force for transferring electrons to anodes.[21,28] Thus, while multiple experiments have shown that biofilm anodes are severely affected by the pH value,[20a,21,26b,c,27] more information related to both the physiological impact (effects on metabolic activity of cells), along with the biochemical and electrochemical effects (changes in cytochrome electron-transfer kinetics), is needed to elucidate the importance of proton export on electron transfer through biofilms to anodes. Independent of the exact mechanism, diffusive proton transport is predicted to result in less active microbes near the biofilm/anode interface that may limit current density and thus the extent of biofilm growth.

Oxidized cytochrome concentration gradient

Within a *Geobacter* biofilm, an oxidized extracellular cytochrome may both accept electrons directly from the microbe it is associated with and from neighboring reduced cytochromes originating from microbes residing farther from the anode surface (Scheme 1). This competition for use of cytochromes is expected to generate a concentration gradient of oxidized cytochromes (and due to mass balance, reduced cytochromes) across the biofilm (Figure 2). In this gradient, cells closer to the anode surface experience a higher concentration of oxidized cytochromes able to accept their electrons, whereas cells farther from the anode surface experience a lower local concentration of oxidized cytochromes able to accept their electrons. As a result, the activity of cells is expected to decrease with increasing distance from the anode surface, opposite the effect expected from the pH gradient described above. In the limiting case, the local concentration of oxidized cytochromes at the outer edge of the biofilm will be too low to support additional biofilm growth. Under this condition, modeling indicates that the biofilm is still predicted to exhibit an undistorted sigmoid-shaped catalytic current–voltage dependency, as has been observed experimentally in many laboratories.[3a,6a,9b,20b]

Three lines of experimental evidence indicate that such a concentration gradient occurs within a *Geobacter* biofilm anode. We (Glaven and Tender) recently obtained direct evidence for such a gradient, in which the electrochemical potential inside a *G. sulfurreducens* biofilm measured 10 μm from the anode surface is approximately −0.2 V versus SHE (Snider, et al., manuscript in preparation). At this potential, cytochromes are over 80% reduced, even though a highly favorable electron acceptor (an anode poised at +0.1 V vs. SHE) is only 10 μm away. Secondly, spectral evidence is provided by Liu and Bond,[8c] in which the proportion of reduced cytochromes within a respiring *Geobacter* biofilm anode increases with increasing biofilm thickness even though cells are again only microns away from an anode poised at a potential sufficiently positive to oxidize all *c*-type cytochromes. Lastly, transcriptional evidence obtained by slicing biofilms and comparing gene expression at the top versus near the electrode[29] revealed down-regulation of acetate oxidation and ribosomal genes, indicating respiration rates slowing with increased distance from the anode.

Role of nanowires

Proteinaceous filaments extending from the cell membrane into the extracellular environment have been observed for many electrode-reducing bacteria.[24b,30] Filamentous structures from two anode-respiring organisms, *G. sulfurreducens*[30,31] and *S. oneidensis*,[23–25,32] have been investigated in depth. Specifically, conductivity across the diameter of sheared *G. sulfurreducens* fibers[30] could be measured by means of conducting atomic force microscopy (AFM), which could not be detected in Type IV pili mutants. Conductivity could also be measured across the diameter and along the length of individual *S. oneidensis* fibers,[23,24b] but aside from mutants in the general Type II secretion pathway responsible for excreting a wide range of proteins to the *Shewanella* outer surface, no data is available on the identity or composition of *Shewanella* fibers. In the case of the lengthwise conductivity measurements, Polizzi et al.[25] calculated that this conductivity could arise from electron superexchange involving redox cofactors associated with the fiber rather than from metallic conductivity.[31,33] Although there are clear differences between these two organisms, the apparent conductivity of both *Geobacter* and *Shewanella* fibers has led to the general term of "nanowires" for these extracellular structures contributing to extracellular electron transport.

The *Geobacter* structures exhibiting this conductivity are believed to be primarily comprised of the Type IV pili structural protein PilA,[30] although other filamentous appendages are present in deletion mutants lacking PilA.[34] All *Geobacter* species, as well as close relatives, which are not capable of electron transfer to electrodes, possess a complete suite of Type IV pili genes typically studied for their ability to retract and pull cells closer to surfaces. The PilA protein of *Geobacter* is also significantly shorter than most commonly studied bacterial Type IV pilins, including those found in *Shewanella*, which has

also been interpreted as evidence that these structures perform additional roles.[35]

Deletion of the entire *pilA* gene significantly inhibits attachment of cells to each other[36] and affects formation of biofilms on glass slides even when electron transfer is not a consideration, further indicating that *Geobacter* pili contribute to adhesion and attachment. PilA mutants also attach poorly to anodes and secrete fewer essential cytochromes such as OmcZ,[35,37] offering a possible explanation for why PilA is required for maximum catalytic current generation.[6c,33] Deletion of the same pilin, however, does not affect electron transfer reactions in which a cathode serves as the electron donor.[38] Further complicating elucidation of the specific role of pili in electron-transport of actively respiring anode grown *Geobacter* biofilms is the fact that the *c*-type cytochrome OmcS has been shown to localize along pili during metal reduction[12c,35] and during interspecies electron transfer between cell aggregates undergoing syntrophic respiration.[39] Moreover, it has been shown that *pilA* contains two different translational start sites, resulting in a long and short isoform of the protein.[40] Expression of only the long form of PilA results in cells unable to produce pili, but rescues much of the cytochrome secretion defects and restores 75% of catalytic current production to *G. sulfurreducens pilA* mutants when grown on anodes.[40]

Despite the confounding effects of pili on attachment, adhesion, retraction, and anchoring of cytochromes, which could all lead to shorter electron transfer distances and increased biofilm growth, a decrease in current generation by *Geobacter pilA* mutants has been attributed to inherent conductive properties of these structures.[31] Temperature-dependency measurements of dried crude pili extracts, and on mutant biofilms that form uniquely tough layers able to be peeled from electrodes and placed across the gap of a split-gold electrode, suggest that direct conduction of electrons through these preparations occurs by a metallic-like process.[31] It is not clear at this time how this data relates to the mechanism controlling the electron transport through an intact, actively respiring wild-type biofilm, and the interpretation of these experiments has been debated elsewhere.[33] However, the hypothesis of metallic electron conduction by pili does not provide explanations for the finite thickness of biofilms, their diffusive redox characteristics, their conductive properties measured while active respiring, or the finding that cytochromes in actively respiring *Geobacter* biofilms are partially reduced.

Conclusions

We have described an evolving scheme of biofilm anode respiration that is ultimately controlled by superexchange among extracellular cytochromes. Although it is likely that other components are also involved, this model is able to account for many different types of experimental evidence reported for actively respiring *Geobacter* biofilm anodes and places specific physical limits on both the thickness and current densities obtainable by anode-reducing bacteria.

According to this concept, local pH values in the biofilm are expected to decrease with increasing biofilm thickness due to the finite rate of outward diffusion of protons generated inside the biofilm by respiration. Low pH values may inhibit the rate cytochromes operate at in superexchange directly by altering redox potentials as well as indirectly by slowing the metabolic activity of the cells they are associated with. In addition, the finite rate of electron exchange between cytochromes is expected to cause the local concentration of oxidized cytochromes in the biofilm to decrease with increasing distance from the anode surface. This phenomenon results from the dual use of oxidized cytochromes to both accept electrons emerging from local cells, and to accept electrons from cells residing farther from the anode surface.

Based on these outcomes, we propose that a biofilm anode will grow in thickness until either the pH value near the anode surface becomes sufficiently low that it inhibits cytochrome function of the innermost cells, thereby limiting the ability of all cells in the biofilm to transfer electrons to the anode, or until the local concentration of oxidized cytochromes experienced by the outermost cells becomes too low to support additional growth. As experiments have directly detected both of these inhibitory effects within living *G. sulfurreducens* biofilm anodes, they likely act synergistically to limit biofilm thickness and thus catalytic activity.

Key challenges that remain are experimental visualization of a network of cytochromes throughout the biofilm and the extracellular structures that ensure the close interactions required for rapid electron transfer. Extrapolating from an entirely different organism, to explain the conductivity measured along a single isolated *Shewanella* fiber,[24a] a superexchange-based mechanism would require cofactor spacing on the order of 1 nm, consistent with intra-heme spacing in multiheme *c*-type cytochromes.[7,23,25] With the identification of at least one multiheme cytochrome that aligns along *Geobacter* pili (OmcS), multiple cytochromes found associated with cell surfaces (e.g., OmcB and OmcE), cytochromes found associated with extracellular materials (OmcZ), and more than 50 genes encoding for additional multiheme cytochromes,[41] numerous candidates for interacting self-exchange pathways exist along cell surfaces and extracellular structures.

Acknowledgements

D.R.B. is supported by the Office of Science (BER), U.S. Department of Energy (DE-SC0006868); S.M.G. and L.M.T. are supported by the Naval Research Laboratory and the Office of Naval Research (N00014-10-WX20463); C.I.T. is supported by the Office of Naval Research (N00014-10M-0231).

Keywords: biofilms · electrochemistry · fuel cells · microbes · nanowires

[1] a) A. E. Franks, K. P. Nevin, *Energies* **2010**, *3*, 899–919; b) D. R. Lovley, *Energy Environ. Sci.* **2011**, *4*, 4896–4906.
[2] A. P. Borole, G. Reguera, B. Ringeisen, Z. W. Wang, Y. J. Feng, B. H. Kim, *Energy Environ. Sci.* **2011**, *4*, 4813–4834.

[3] a) E. Marsili, J. B. Rollefson, D. B. Baron, R. M. Hozalski, D. R. Bond, *Appl. Environ. Microbiol.* **2008**, *74*, 7329 – 7337; b) E. Marsili, J. Sun, D. R. Bond, *Electroanalysis* **2010**, *22*, 865 – 874.

[4] C. I. Torres, A. K. Marcus, H. S. Lee, P. Parameswaran, R. Krajmalnik-Brown, B. E. Rittmann, *FEMS Microbiol. Rev.* **2010**, *34*, 3 – 17.

[5] a) K. Rabaey, P. Girguis, L. K. Nielsen, *Curr. Opin. Biotechnol.* **2011**, *22*, 371 – 377; b) P. R. Girguis, M. E. Nielsen, I. Figueroa, *Curr. Opin. Biotechnol.* **2010**, *21*, 252 – 258; c) J. J. Fornero, M. Rosenbaum, L. T. Angenent, *Electroanalysis* **2010**, *22*, 832 – 843.

[6] a) K. Fricke, F. Harnisch, U. Schröder, *Energy Environ. Sci.* **2008**, *1*, 144 – 147; b) S. Srikanth, E. Marsili, M. C. Flickinger, D. R. Bond, *Biotechnol. Bioeng.* **2008**, *99*, 1065 – 1073; c) H. Richter, K. P. Nevin, H. Jia, D. A. Lowy, D. R. Lovley, L. M. Tender, *Energy Environ. Sci.* **2009**, *2*, 506 – 516; d) S. M. Strycharz-Glaven, L. M. Tender, *ChemSusChem* **2012**, *5*, 1106 – 1118.

[7] S. M. Strycharz-Glaven, R. M. Snider, A. Guiseppi-Elie, L. M. Tender, *Energy Environ. Sci.* **2011**, *4*, 4366 – 4379.

[8] a) A. Jain, G. Gazzola, A. Panzera, M. Zanoni, E. Marsili, *Electrochim. Acta* **2011**, *56*, 10776 – 10785; b) Y. Liu, H. Kim, R. R. Franklin, D. R. Bond, *ChemPhysChem* **2011**, *12*, 2235 – 2241; c) Y. Liu, D. R. Bond, *ChemSusChem* **2012**, *5*, 1047 – 1053.

[9] a) A. J. Bard, L. R. Faulkner, *Electrochemical Methods: Fundamentals and Applications, 2nd ed.*, Wiley, New York, **2001**; b) S. M. Strycharz, A. P. Malanoski, R. M. Snider, H. Yi, D. R. Lovley, L. M. Tender, *Energy Environ. Sci.* **2011**, *4*, 896 – 913.

[10] a) E. F. Dalton, N. A. Surridge, J. C. Jernigan, K. O. Wilbourn, J. S. Facci, R. W. Murray, *Chem. Phys.* **1990**, *141*, 143 – 157; b) I. Katakis, A. Heller, *Anal. Chem.* **1992**, *64*, 1008 – 1013; c) R. Forster, D. Walsh, N. Mano, F. Mao, A. Heller, *Langmuir* **2004**, *20*, 862 – 868.

[11] a) K. Inoue, X. Qian, L. Morgado, B.-C. Kim, T. Mester, M. Izallalen, C. A. Salgueiro, D. R. Lovley, *Appl. Environ. Microbiol.* **2010**, *76*, 3999 – 4007; b) X. L. Qian, T. Mester, L. Morgado, T. Arakawa, M. L. Sharma, K. Inoue, C. Joseph, C. A. Salgueiro, M. J. Maroney, D. R. Lovley, *Biochim. Biophys. Acta Bioenerg.* **2011**, *1807*, 404 – 412; c) M. Pessanha, Y. Y. Londer, W. C. Long, J. Erickson, P. R. Pokkuluri, M. Schiffer, C. A. Salgueiro, *Biochemistry* **2004**, *43*, 9909 – 9917.

[12] a) Y. H. R. Ding, K. K. Hixson, C. S. Giometti, A. Stanley, A. Esteve-Núñez, T. Khare, S. L. Tollaksen, W. H. Zhu, J. N. Adkins, M. S. Lipton, R. D. Smith, T. Mester, D. R. Lovley, *Biochim. Biophys. Acta Proteins Proteomics* **2006**, *1764*, 1198 – 1206; b) Y. H. R. Ding, K. K. Hixson, M. A. Aklujkar, M. S. Lipton, R. D. Smith, D. R. Lovley, T. Mester, *Biochim. Biophys. Acta Proteins Proteomics* **2008**, *1784*, 1935 – 1941; c) C. Leang, X. Qian, T. Mester, D. R. Lovley, *Appl. Environ. Microbiol.* **2010**, *76*, 4080 – 4084; d) C. Leang, M. V. Coppi, D. R. Lovley, *J. Bacteriol.* **2003**, *185*, 2096 – 2103; e) T. Mehta, M. V. Coppi, S. E. Childers, D. R. Lovley, *Appl. Environ. Microbiol.* **2005**, *71*, 8634 – 8641; f) J. B. Rollefson, C. S. Stephen, M. Tien, D. R. Bond, *J. Bacteriol.* **2011**, *193*, 1023 – 1033; g) X. L. Qian, G. Reguera, T. Mester, D. R. Lovley, *FEMS Microbiol. Lett.* **2007**, *277*, 21 – 27.

[13] J. Simon, R. J. M. van Spanning, D. J. Richardson, *Biochim. Biophys. Acta Bioenerg.* **2008**, *1777*, 1480 – 1490.

[14] a) R. S. Hartshorne, B. N. Jepson, T. A. Clarke, S. J. Field, J. Fredrickson, J. Zachara, L. Shi, J. N. Butt, D. J. Richardson, *J. Biol. Inorg. Chem.* **2007**, *12*, 1083 – 1094; b) R. S. Hartshorne, C. L. Reardon, D. Ross, J. Nuester, T. A. Clarke, A. J. Gates, P. C. Mills, J. K. Fredrickson, J. M. Zachara, L. Shi, A. S. Beliaev, M. J. Marshall, M. Tien, S. Brantley, J. N. Butt, D. J. Richardson, *Proc. Natl. Acad. Sci. USA* **2009**, *106*, 22169 – 22174; c) T. A. Clarke, M. J. Edwards, A. J. Gates, A. Hall, G. F. White, J. Bradley, C. L. Reardon, L. Shi, A. S. Beliaev, M. J. Marshall, Z. M. Wang, N. J. Watmough, J. K. Fredrickson, J. M. Zachara, J. N. Butt, D. J. Richardson, *Proc. Natl. Acad. Sci. USA* **2011**, *108*, 9384 – 9389.

[15] a) J. P. Busalmen, A. Esteve-Núñez, A. Berna, J. M. Feliu, *Bioelectrochemistry* **2010**, *78*, 25 – 29; b) A. Esteve-Núñez, J. P. Busalmen, A. Berna, C. Gutierrez-Garran, J. M. Feliu, *Energy Environ. Sci.* **2011**, *4*, 2066 – 2069.

[16] D. Millo, F. Harnisch, S. A. Patil, H. K. Ly, U. Schröder, P. Hildebrandt, *Angew. Chem.* **2011**, *123*, 2673 – 2675; *Angew. Chem. Int. Ed.* **2011**, *50*, 2625 – 2627.

[17] a) B.-C. Kim, D. R. Lovley, *FEMS Microbiol. Lett.* **2008**, *286*, 39 – 44; b) B. C. Kim, X. L. Qian, L. A. Ching, M. V. Coppi, D. R. Lovley, *J. Bacteriol.* **2006**, *188*, 3138 – 3142.

[18] K. Inoue, C. Leang, A. E. Franks, T. L. Woodard, K. P. Nevin, D. R. Lovley, *Environ. Microbiol. Rep.* **2011**, *3*, 211 – 217.

[19] B.-C. Kim, B. L. Postier, R. J. DiDonato, S. K. Chaudhuri, K. P. Nevin, D. R. Lovley, *Bioelectrochemistry* **2008**, *73*, 70 – 75.

[20] a) C. I. Torres, A. Kato Marcus, B. E. Rittmann, *Biotechnol. Bioeng.* **2008**, *100*, 872 – 881; b) C. I. Torres, A. K. Marcus, P. Parameswaran, B. E. Rittmann, *Environ. Sci. Technol.* **2008**, *42*, 6593 – 6597.

[21] K. P. Katuri, P. Kavanagh, S. Rengaraj, D. Leech, *Chem. Commun.* **2010**, *46*, 4758 – 4760.

[22] a) R. Mahadevan, D. R. Bond, J. E. Butler, A. Esteve-Nuñez, M. V. Coppi, B. O. Palsson, C. H. Schilling, D. R. Lovley, *Appl. Environ. Microbiol.* **2006**, *72*, 1558 – 1568; b) A. Esteve-Nuñez, M. Rothermich, M. Sharma, D. R. Lovley, *Environ. Microbiol.* **2005**, *7*, 641 – 648.

[23] M. Y. El-Naggar, G. Wanger, K. M. Leung, T. D. Yuzvinsky, G. Southam, J. Yang, W. M. Lau, K. H. Nealson, Y. A. Gorby, *Proc. Natl. Acad. Sci. USA* **2010**, *107*, 18127 – 18131.

[24] a) M. El-Naggar, Y. Gorby, W. Xia, *Biophys. J.* **2008**, *95*, L10 – L12; b) Y. A. Gorby, S. Yanina, J. S. McLean, K. M. Rosso, D. Moyles, A. Dohnalkova, T. J. Beveridge, I. S. Chang, B. H. Kim, K. S. Kim, D. E. Culley, S. B. Reed, M. F. Romine, D. A. Saffarini, E. A. Hill, L. Shi, D. A. Elias, D. W. Kennedy, G. Pinchuk, K. Watanabe, S. Ishii, B. Logan, K. H. Nealson, J. K. Fredrickson, *Proc. Natl. Acad. Sci. USA* **2006**, *103*, 11358 – 11363.

[25] N. F. Polizzi, S. S. Skourtis, D. N. Beratan, *Faraday Discuss.* **2012**, *155*, 43 – 62.

[26] a) A. K. Marcus, C. I. Torres, B. E. Rittmann, *Electrochim. Acta* **2010**, *55*, 6964 – 6972; b) A. K. Marcus, C. I. Torres, B. E. Rittmann, *Bioresour. Technol.* **2011**, *102*, 253 – 262; c) C. Picioreanu, M. C. M. van Loosdrecht, T. P. Curtis, K. Scott, *Bioelectrochemistry* **2010**, *78*, 8 – 24.

[27] A. E. Franks, K. Nevin, H. Jia, M. Izallalen, T. Woodard, D. Lovley, *Energy Environ. Sci.* **2009**, *2*, 113 – 119.

[28] S. A. Patil, F. Harnisch, C. Koch, T. Hübschmann, I. Fetzer, A. A. Carmona-Martínez, S. Müller, U. Schröder, *Bioresour. Technol.* **2011**, *102*, 9683 – 9690.

[29] A. E. Franks, K. P. Nevin, R. H. Glaven, D. R. Lovley, *ISME J.* **2010**, *4*, 509 – 519.

[30] G. Reguera, K. D. McCarthy, T. Mehta, J. S. Nicoll, M. T. Tuominen, D. R. Lovley, *Nature* **2005**, *435*, 1098 – 1101.

[31] N. S. Malvankar, M. Vargas, K. P. Nevin, A. E. Franks, C. Leang, B. C. Kim, K. Inoue, T. Mester, S. F. Covalla, J. P. Johnson, V. M. Rotello, M. T. Tuominen, D. R. Lovley, *Nat. Nanotechnol.* **2011**, *6*, 573 – 579.

[32] A. A. Carmona-Martinez, F. Harnisch, L. A. Fitzgerald, J. C. Biffinger, B. R. Ringeisen, U. Schröder, *Bioelectrochemistry* **2011**, *81*, 74 – 80.

[33] S. M. Strycharz-Glaven, L. M. Tender, *Energy Environ. Sci.* **2012**, 5, 6250 – 6255.

[34] A. Klimes, A. E. Franks, R. H. Glaven, H. Tran, C. L. Barrett, Y. Qiu, K. Zengler, D. R. Lovley, *FEMS Microbiol. Lett.* **2010**, *310*, 62 – 68.

[35] D. L. Cologgi, S. Lampa-Pastirk, A. M. Speers, S. D. Kelly, G. Reguera, *Proc. Natl. Acad. Sci. USA* **2011**, *108*, 15248 – 15252.

[36] G. Reguera, R. B. Pollina, J. S. Nicoll, D. R. Lovley, *J. Bacteriol.* **2007**, *189*, 2125 – 2127.

[37] K. P. Nevin, B. C. Kim, R. H. Glaven, J. P. Johnson, T. L. Woodard, B. A. Methe, R. J. Didonato, S. F. Covalla, A. E. Franks, A. Liu, D. R. Lovley, *PLoS One* **2009**, *4*, e5628.

[38] S. M. Strycharz, R. H. Glaven, M. V. Coppi, S. M. Gannon, L. A. Perpetua, A. Liu, K. P. Nevin, D. R. Lovley, *Bioelectrochemistry* **2011**, *80*, 142 – 150.

[39] Z. M. Summers, H. E. Fogarty, C. Leang, A. E. Franks, N. S. Malvankar, D. R. Lovley, *Science* **2010**, *330*, 1413 – 1415.

[40] L. V. Richter, S. J. Sandler, R. M. Weis, *J. Bacteriol.* **2012**, DOI: 10.1128/JB.06366-11.

[41] B. A. Methé, K. E. Nelson, J. A. Eisen, I. T. Paulsen, W. Nelson, J. F. Heidelberg, D. Wu, M. Wu, N. Ward, M. J. Beanan, R. J. Dodson, R. Madupu, L. M. Brinkac, S. C. Daugherty, R. T. DeBoy, A. S. Durkin, M. Gwinn, J. F. Kolonay, S. A. Sullivan, D. H. Haft, J. Selengut, T. M. Davidsen, N. Zafar, O. White, B. Tran, C. Romero, H. A. Forberger, J. Weidman, H. Khouri, T. V. Feldblyum, T. R. Utterback, S. E. Van Aken, D. R. Lovley, C. M. Fraser, *Science* **2003**, *302*, 1967 – 1969.

Received: November 21, 2011
Revised: December 14, 2011

